AD-A044 239   PRATT AND WHITNEY AIRCRAFT GROUP WEST PALM BEACH FLA --ETC F/G 21/5
APPLICATION OF FRACTURE MECHANICS AT ELEVATED TEMPERATURES.(U)
APR 77   R M WALLACE, C G ANNIS, D L SIMS   F33615-75-C-5097
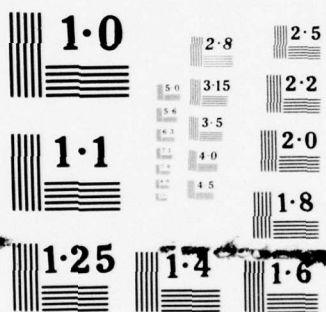UNCLASSIFIED   FR-8100   AFML-TR-76-176-PT-2   NL

1 OF 1
ADA
044239

END
DATE
FILMED
10-77
DDC

AFML-TR-76-176 PART II

20

# APPLICATION OF FRACTURE MECHANICS AT ELEVATED TEMPERATURES

Raymond M. Wallace
Charles G. Annis, Jr.
David L. Sims

United Technologies Corporation
Pratt & Whitney Aircraft Group
Government Products Division
West Palm Beach, Florida 33402

AIR FORCE MATERIALS LABORATORY
AIR FORCE WRIGHT AERONAUTICAL LABORATORIES
AIR FORCE SYSTEMS COMMAND
WRIGHT-PATTERSON AIR FORCE BASE, OHIO 45433
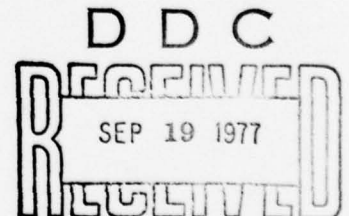
NOTICE

When Government drawings, specifications, or other data are used for any purpose other than in connection with a definitely related Government procurement operation, the United States Government thereby incurs no responsibility nor any obligation whatsoever; and the fact that the government may have formulated, furnished, or in any way supplied the said drawings, specifications, or other data, is not to be regarded by implication or otherwise as in any manner licensing the holder or any other person or corporation, or conveying any rights or permission to manufacture, use, or sell any patented invention that may in any way be related thereto.
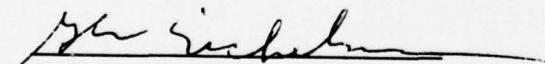
This report has been reviewed by the Information Office (ASD/OIP) and is releasable to the National Technical Information Service (NTIS). At NTIS, it will be releasable to the general public, including foreign nations.

This technical report has been reviewed and is approved for publication.

W. H. REIMANN
Project Engineer

FOR THE DIRECTOR

GAIL E. EICHELMANN, Chief,
Metals Behavior Branch
Metals & Ceramics Division

Copies of this report should not be returned unless return is required by security considerations, contractural obligations, or notice on a specific document.

H38070

REPORT DOCUMENTATION PAGE	READ INSTRUCTIONS BEFORE COMPLETING FORM

1. REPORT NUMBER	2. GOVT ACCESSION NO.	3. RECIPIENT'S CATALOG NUMBER
AFML-TR-76-176, Part II		

4. TITLE *(and Subtitle)*
APPLICATION OF FRACTURE MECHANICS AT ELEVATED TEMPERATURES

5. TYPE OF REPORT & PERIOD COVERED
Final Report

6. PERFORMING ORG. REPORT NUMBER
FR-8100

7. AUTHOR(s)
R. M. Wallace, C. G. Annis, Jr., D. L. Sims

8. CONTRACT OR GRANT NUMBER(s)
F33615-75-C-5097

9. PERFORMING ORGANIZATION NAME AND ADDRESS
Pratt & Whitney Aircraft Group
Government Products Division

10. PROGRAM ELEMENT, PROJECT, TASK AREA & WORK UNIT NUMBERS

11. CONTROLLING OFFICE NAME AND ADDRESS
Air Force Materials Laboratory
Air Force Systems Command
Wright-Patterson AFB, Ohio 45433

12. REPORT DATE
April 1977

13. NUMBER OF PAGES
63   266 p.

14. MONITORING AGENCY NAME & ADDRESS *(if different from Controlling Office)*
Air Force Materials Laboratory
Air Force Systems Command
Wright-Patterson AFB, Ohio 45433

15. SECURITY CLASS. *(of this report)*
Unclassified

15a. DECLASSIFICATION/DOWNGRADING SCHEDULE

16. DISTRIBUTION STATEMENT *(of this Report)*

Approved for public release, distribution unlimited.

DDC
RECEIVED
SEP 19 1977
B

17. DISTRIBUTION STATEMENT *(of the abstract entered in Block 20, if different from Report)*

18. SUPPLEMENTARY NOTES

19. KEY WORDS *(Continue on reverse side if necessary and identify by block number)*

Fracture Mechanics,	Life Predictions
IN-100,	
Interpolative Model,	
Crack Propagation,	
Hyperbolic Sine,	

20. ABSTRACT *(Continue on reverse side if necessary and identify by block number)*

The applicability of linear elastic fracture mechanics to predict crack growth at elevated temperatures is investigated. The interactive effects of stress, temperature, time, and environment on the crack growth of an advanced gas turbine disk alloy, IN-100, are described with an interpolative empirical model based on the hyperbolic sine.

392887

FOREWORD

CONTENTS

iii

ILLUSTRATIONS

SUMMARY

This report investigates the applicability of linear elastic fracture mechanics to predict crack growth at elevated temperatures. The interactive effects of stress, temperature, time, and environment on the crack growth process of an advanced gas turbine disk alloy, IN-100, are investigated. The effects are described with an interpolative empirical model based on the hyperbolic sine.

SECTION I
INTRODUCTION

It has been estimated that replacement costs for Low-Cycle Fatigue (LCF) limited engine disk components could reach the $100,000,000 level by 1980 to 1985 (Reference 1). A tremendous cost savings could be realized if a procedure was developed to provide accurate assessment of useful residual life in retired engine disks (Reference 2). This procedure is based on improved inspection and fracture mechanics life prediction techniques. This report addresses the development of advanced fracture mechanics concepts for the prediction of crack growth at elevated temperatures. The results of this program will be used in conjunction with advanced inspection techniques for residual life predictions of retired turbine disks (Reference 3).

1

SECTION II
APPLICABILITY OF LINEAR ELASTIC FRACTURE MECHANICS
AT ELEVATED TEMPERATURES

All fracture mechanics evaluations were performed on GATORIZED™ IN-100, an advanced nickel-base turbine disk alloy used in the F100 turbofan engine. Specimens specifically designated to this contract were machined from heat BANQ-499, but a significant amount of crack propagation data existed for this alloy prior to the start of this program. These data are also used in the analyses. Heat-treatment consists of solutionization at 2050°F, stabilization at 1600 and 1800°F, and precipitation hardening at 1200 and 1400°F. Typical chemical composition is 0.07C-12.4Cr-18.5Co-3.2Mo-4.32Ti-4.98Al-0.78V-0.02B-0.06Zr - balance nickel. When super-plastically forged with the GATORIZED forging process, IN-100 becomes a fine-grain (ASTM 12-14), isotropic material.

Tensile, stress rupture, and creep test results for two forgings from this heat (499-A2A and 499-A2B) are given in Table 1.

TABLE 1. MECHANICAL PROPERTIES OF TWO IN-100 PANCAKE FORGINGS

		Tensile Properties			
Disk No.	Temp (°F)	Yield Strength (ksi)	Ultimate Tensile Strength (ksi)	EL %	RA %
499-A2A	RT	164.5	232.4	22.0	22.2
499-A2A	1300	157.2	177.0	14.0	22.3
499-A2B	RT	164.9	232.0	22.0	21.5
499-A2B	1300	156.0	179.1	14.7	16.4

		Stress Rupture Properties			
Disk No.	Temp (°F)	Stress (ksi)	Life (hr)	EL %	RA %
499-A2A	1350	95	28.0	10.6	15.9
499-A2B	1350	95	18.0	8.1	15.6
499-A2B	1350	95	19.5	8.0	8.2
499-A2B	1350	95	19.3	6.7	12.9

		Creep Rupture Properties			
Disk No.	Temp (°F)	Stress (ksi)	0.1% (hr)	0.2% (hr)	Total Life (hr)
499-A2A	1300	80	—	175.5	233.2*
499-A2B	1300	80	114.5	142.5	143.2*

*Test Discontinued.

The usefulness of Linear Elastic Fracture Mechanics (LEFM) depends on a uniparametrical connection between crack growth rate and the stress intensity factor. Our general approach is to first determine the limits of applicability of LEFM concepts at elevated temperatures.

Recently, a number of investigators have attempted to determine the relevance of linear elastic fracture mechanics as applied to crack growth at elevated temperatures (References 4 and 5). In most cases, crack growth rate could successfully be expressed in term of the stress intensity factor, K (Reference 4); however, some work showed better correlations with net section stress or with some reference stress state (Reference 5). In general, the higher strength low ductility alloys correlated better with K and the lower strength high ductility alloys correlated with net section stress.

It has been postulated that the inadequacy of linear elastic concepts for correlating crack growth rate data with the stress intensity factor, K, may be due to the nonlinearity of constitutive laws for the immediate vicinity of the crack tip. Because of the success of applying the J contour integral to describe the singular terms of stress or strain for a nonlinear elastic material, the applicability of J to creep crack growth has been investigated (References 5 and 6). Experimental results show that creep crack growth for ductile alloys can be approximated by $\dot{J}$, the potential power release rate. Another approach developed the C* parameter, an energy rate line integral, to characterize the crack tip stress and strain rate field (Reference 7). The problem of analytically calculating C* for a crack in a real structure is somewhat complicated. Research continues in this area.

Fortunately, experience has shown that linear elastic fracture mechanics is generally applicable to high strength gas turbine alloys (Reference 4). The hostile environment of the gas turbine engine can have a significant role in embrittling the crack tip region, reducing large scale inelasticity. It has been shown that grain boundary oxidation (References 4 and 8) affects the rate of intergranular crack propagation. The structure of the material in front of the crack tip is altered. Not only is the immediate vicinity of the tip oxidized, the region ahead of the crack is depleted of oxide forming elements. Thus, there are two relevant spheres of local damage: (1) the inelastic zone associated with local creep deformation and cyclic plasticity and (2) the zone that is locally fractured because of oxidation. The problem then becomes one of comparative kinetics. If oxidation generally prevails over creep, then the crack tip will respond elastically and LEFM is applicable. The dominance of large scale inelasticity, however, necessitates inelastic fracture criteria.

In this task, specimen geometries, specimen thicknesses, stress-crack length combinations, and net section stresses were varied to test the uniparametrical relation between crack growth rate and applied stress intensity. In general, when crack tip nonlinearity is small compared to elastic crack tip stress fields, linear elastic fracture mechanics concepts are applicable.

The specimens selected for this phase of the program include the modified compact tension (Figure 1) and through-thickness center-crack (Figure 2) geometries.

Test specimens are precracked using procedures outlined in ASTM E-399. Precracking is generally performed at room temperature; anomalous precracking effects are easily recognizable.

Crack propagation testing is conducted on closed-loop servocontrolled equipment under load control. Cyclic tests are performed using isosceles triangular load waveforms. Load ramping rates for the mission mix crack propagation tests are closely controlled and monitored for benefit of subsequent modeling. Unless noted otherwise, specimens are heated using resistance, clamshell furnaces.

Crack lengths are measured directly with a traveling microscope with the cyclic load removed, holding the specimen at the mean stress level. This procedure holds the specimen rigid while opening the crack slightly to make the crack tip more visible. A high-intensity light is used at an oblique angle to the crack to provide illumination and a higher degree of crack tip detection. On tests at elevated temperatures, the furnace is removed from the specimen in order to facilitate optical measurement.

An attempt is made to measure crack growth in increments no larger than 0.020-inch. Crack length measurements are considered to be accurate to within ± 0.001-inch.

Specimen test conditions are summarized in table 2.
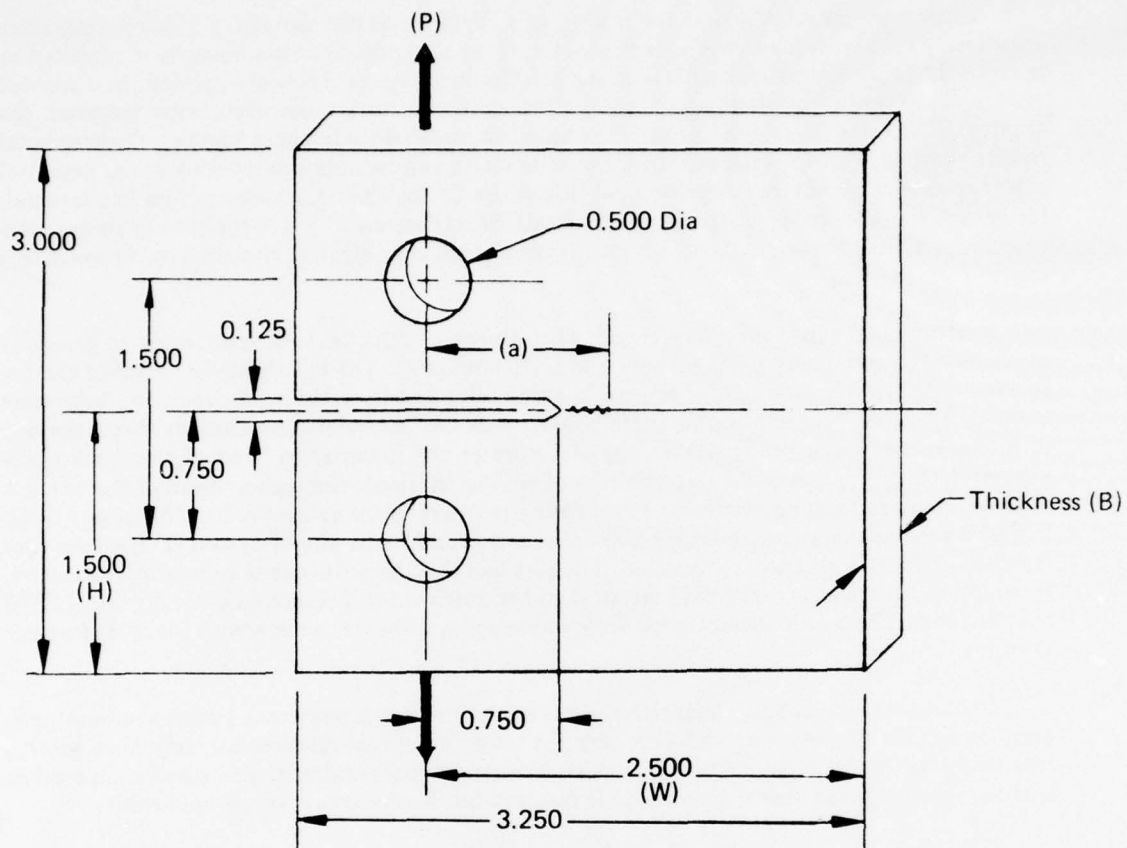
K Calibration:

$$K = Y \frac{P}{BW} \sqrt{a}$$

For a/w = 0.3 − 0.7; H/W = 0.6

$$Y = f(a/w) = [0.2960 - 1.855\,(a/w) + 6.557\,(a/w)^2$$
$$- 10.17\,(a/w)^3 + 6.389\,(a/w)^4]\ 10^2$$

Accuracy: 0.5%

Net Section Stress:

$$\sigma_{Net} = \frac{KW^{1/2}}{f(a/w)(w\text{-}a)} \left[1 + \frac{3(w+a)}{(w-a)} \right]$$

FD 82803A

Figure 1. Modified Compact Tension Specimen

4

σ

B

H

2A

H

B′ B′

W

σ
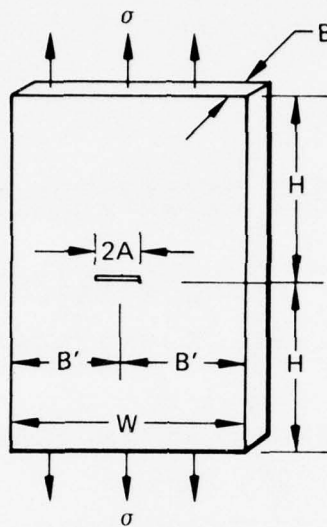
K Calibration:

$$K = Y \, \sigma \sqrt{\pi A}$$

$$Y = F \, (A/B') = [1 - 0.025 \, (A/B')^2 + 0.06 \, (A/B')^4] \, \sec \sqrt{\frac{\pi A}{2B'}}$$

Accuracy = 0.1% for any A/B

Net Section Stress:

$$\sigma_{Net} = Load/B(W\text{-}2A)$$

FD 82804A

Figure 2. Center Crack Specimen

TABLE 2. CRACK PROPAGATION TESTING OF IN-100 (PWA 1073)

Program Phase/Tasks	Specimen Number	Temp. (°F)	Specimen Type	Nominal Thickness	Cyclic Frequency	Stress Ratio	K_i ksi·$\sqrt{in}$	a_i in.	$\sigma_{net\,i}$ (ksi)	Curvature* (%)
1/6, 1, 2	601	1200	MCT	0.125	20 cps	0.5	20	0.8	20.8	N/A
1/5, 1, 2, 6	602	1200	MCT	0.250	2-min dwell	0.1	20	0.8	20.8	N/A
1/6, 1, 2	603	1200	MCT	0.125	20 cps	0.5	20	1.1	48.4	N/A
1/4, 1, 2	604	1200	MCT	0.250	0.5 cps	0.1	30	1.1	36.3	N/A
1/4, 1, 2	605	1200	MCT	0.250	0.5 cpm	0.1	20	0.8	21.4	N/A
1/5, 1, 6	606	1200	MCT	0.125	2-min dwell	0.1	35	1.2	46.0	N/A
1/6, 1	607	1200	MCT	0.250	0.5 cpm	0.5	30	1.1	35.6	N/A
1/6, 4	608	1200	MCT	0.250	0.5 cpm	0.5	31	1.1	37.9	N/A
2/1	609	1200	MCT	0.230	5-min dwell	0.1	21	0.9	23.3	N/A
2/1	610	1200	MCT	0.210	5-min dwell	0.1	30	1.1	36.5	7.0
2/1	612	1200	MCT	0.250	20-min dwell	0.1	20	0.9	22.4	8.5
1/5	613	1350	MCT	0.250	20-min dwell	0.1	30	1.1	37.7	13.0
2/1	614	1200	MCT	0.250	20-min dwell	0.1	30	0.9	33.9	11.0
1/6, 1	616	1350	MCT	0.125	20 cps	0.5	15	0.8	16.3	N/A
1/4	617	1200	MCT	0.125	1 cps	0.1	21	0.8	21.7	N/A
1/4, 6	618	1200	MCT	0.125	20 cps	0.1	VOID - Accidental Overload			
1/3	620	1200/1350	MCT	0.250	10 cpm	0.1	16	0.9	17.4	N/A
1/4, 6	622	1200	MCT	0.250	20 cps	0.8	22	0.9	24.1	N/A
1/2, 5	624	1200	CF	0.125	10 cpm	0.1	40	0.05	105.7	16.0
1/3	627	1350/1200	MCT	0.250	10 cpm	0.5	16	0.8	17.9	N/A
1/3	628	1400/1200	MCT	0.250	10 cpm	0.1	16	0.8	18.2	N/A
1/2, 5	645	1200	CF	0.125	2-min dwell	0.1	43	0.06	107.3	10.0
1/2, 5	646	1350	CF	0.125	10 cpm	0.1	35	0.04	99.9	N/A
1/2, 5	647	1350	CF	0.125	20-min dwell	0.1	44	0.06	108.7	48.0
1/2, 5	648	1200	CF	0.125	20-min dwell	0.1	45	0.07	106.5	30.0
2/2, 5	684	1200	CF	0.120	2-min dwell	0.1	22	0.04	63.5	N/A
2/1	621	1350	MCT	0.250	mix mission	0.1	20	0.9	22.4	N/A
2/1	625	1200	MCT	0.250	mix mission	0.1	20	0.9	22.7	N/A
2/1	626	1350	MCT	0.250	mix mission	0.1	20	0.9	21.7	7.5
2/1	629	1350	MCT	0.250	mix mission	0.1	21	0.8	24.1	N/A
2/1	630	1200	MCT	0.250	mix mission	0.5	22	0.8	25.5	N/A
2/1	631	1350	MCT	0.250	mix mission	0.5	20	0.9	22.9	N/A
2/3	632	1350	MCT	0.250	mix mission	NA	25	0.9	29.9	10.0
2/3	634	1200	MCT	0.250	mix mission	NA	32	0.9	35.3	N/A
2/1	660	1200	MCT	0.250	20-min dwell	0.1	15	0.8	16.2	N/A
2/3	661	1350	MCT	0.250	mix mission	0.8	16	0.8	17.1	N/A
2/3	662	1350	MCT	0.250	mix mission	0.8	16	0.9	17.4	N/A
2/4	663	1350	MCT	0.250	mix mission	Invalid Test				
2/4	664	1350	MCT	0.250	mix mission	0.8	16	0.8	16.4	N/A
2/3	665	1350	MCT	0.250	mix mission	0.1	16	0.9	17.7	N/A
2/3	666	1200	MCT	0.250	mix mission	0.1	16	0.8	16.6	N/A
2/3	667	1200	MCT	0.250	mix mission	N/A	19	1.0	21.0	N/A
2/3	669	1200	MCT	0.250	mix mission	0.1	15	0.8	16.1	N/A
2/3	670	1200	MCT	0.251	mix mission	0.5	16	0.9	17.1	N/A
2/3	671	1200	MCT	0.250	mix mission	0.5	16	0.9	16.6	N/A
2/1	686	1200	MCT	0.850	sustained load	N/A	16	0.8	38.8	N/A

*N/A indicates less than 5% curvature.

6

TABLE 2. CRACK PROPAGATION TESTING OF IN-100 (PWA 1073) (CONTINUED)

Program Phase/Task	Specimen Number	Temp (°F)	Specimen Type	Nominal Thickness	Cyclic Frequency	Stress Ratio	Mission Variables K_i ($ksi\sqrt{in.}$)	a_i (in.)	σnet_i (ksi)	Curvature* (%)
1/4, 6	619	1350	MCT	0.125	20 cps	0.8	37	0.8	38.8	NA
1/4, 6	623	1350	MCT	0.125	10 cpm	0.8	26	0.8	27.2	NA
1/3	627	1350/1200	MCT	0.250	10 cpm	0.1	16	0.8	17.9	NA
1/3, 4, 6	633	1200	MCT	0.250	10 cpm	0.1	16	1.0	18.6	NA
1/3, 4, 6	635	1100	MCT	0.250	2 cpm	0.3	21	0.9	23.7	NA
1/3, 4, 6	636	1200	MCT	0.125	10 cpm	0.1	21	0.8	22.0	NA
1/3, 4	637	1300	MCT	0.125	10 cpm	0.1	21	0.8	23.0	NA
1/3, 4	638	1200	MCT	0.125	10 cpm	0.1	21	0.8	22.0	NA
1/3, 4	639	1050	MCT	0.125	10 cpm	0.1	16	0.9	19.0	NA
1/3, 4, 6	640	1200	MCT	0.125	10 cpm	0.1	21	0.8	21.8	NA
1/3, 4	641	1000	MCT	0.125	10 cpm	0.1	21	0.8	21.8	NA
1/3, 4	642	1000	MCT	0.125	10 cpm	0.1	21	0.8	21.6	NA
1/3, 4	644	1200	MCT	0.100	20 cps	0.1	26	0.8	29.0	NA
1/2, 3, 5	649	1200	CF	0.125	2 min dwell	0.1	39	0.06	101.2	11
1/5	668	1000	MCT	0.250	2 min dwell	0.1	21	0.8	21.5	NA
2/3	673	1200	MCT	0.250	mix mission	0.8	21	0.8	22.5	NA
2/4	674	1200	MCT	0.250	mix mission	0.5	31	0.8	32.6	NA
2/3	675	1200	MCT	0.250	mix mission	0.5	16	0.8	36.5	NA
2/3	676	1200	MCT	0.250	mix mission	0.5	22	0.9	23.0	NA
1/5	677	1200	MCT	0.250	10 min dwell	0.1	25	0.8	26.8	NA
2/3	678	1350	MCT	0.250	mix mission	0.5	16	-	-	Invalid Test
2/3	679	1350	MCT	0.250	mix mission	0.5	16	0.8	16.6	NA
2/3	680	1200	MCT	0.250	mix mission	0.5	21	0.9	22.6	NA
2/3	681	1350	MCT	0.250	mix mission	0.5	16	0.9	17.1	NA
1/1, 2, 4	682	1300	MCT	0.250	mix mission	0.1	21.4	0.9	23.0	NA
2/1	683	1200	MCT	0.250	mix mission	0.1	21	0.8	22.3	NA
1/1, 2	685	1200	MCT	0.850	10 cpm	0.1	16	0.8	16.2	NA
1/5	687	1200	MCT	0.850	10 min dwell	0.1	16	0.8	16.1	NA
1/1, 2	696	1100	MCT	0.250	2 cpm	0.3	23	0.9	27.0	NA

*N/A indicates less than 5% curvature.

EFFECT OF SPECIMEN THICKNESS

Room Temperature

Figure 3 compares crack growth rates in IN-100 for specimens of varying thicknesses at room temperature, R = 0.1. At room temperature, the crack propagation mechanism is predominantly planar slip at low applied stress intensities and multiple slip at high applied stress intensities (Reference 9). In thin sections, crack tip inelasticity (plasticity) increases with increasing stress intensity until the zone size becomes comparable to the specimen thickness. At this point, crack tip plane strain constraint relaxes and crack propagation becomes mixed mode (MODE I and MODE III). For a constant applied stress intensity, mixed mode propagation rates are slower than those for plane strain. The maximum stress intensity at first indication of an observable shear lip (mixed mode) is given in figures 4 and 5 as a function of specimen thickness for IN-100 at room temperature. Note that a ½-inch thick section would not guarantee plane strain conditions for typical applications at room temperature. In order to determine valid K_{Ic} values per ASTM E399, specimens with thicknesses greater than two inches would be required. The room temperature fracture toughness (K_{Ic}) of IN-100 as determined by J-Integral techniques is 143 ksi$\sqrt{in.}$ (Reference 10).

In summary, linear elastic fracture mechanics concepts are not generally applicable to the prediction of crack growth in IN-100 at room temperature.
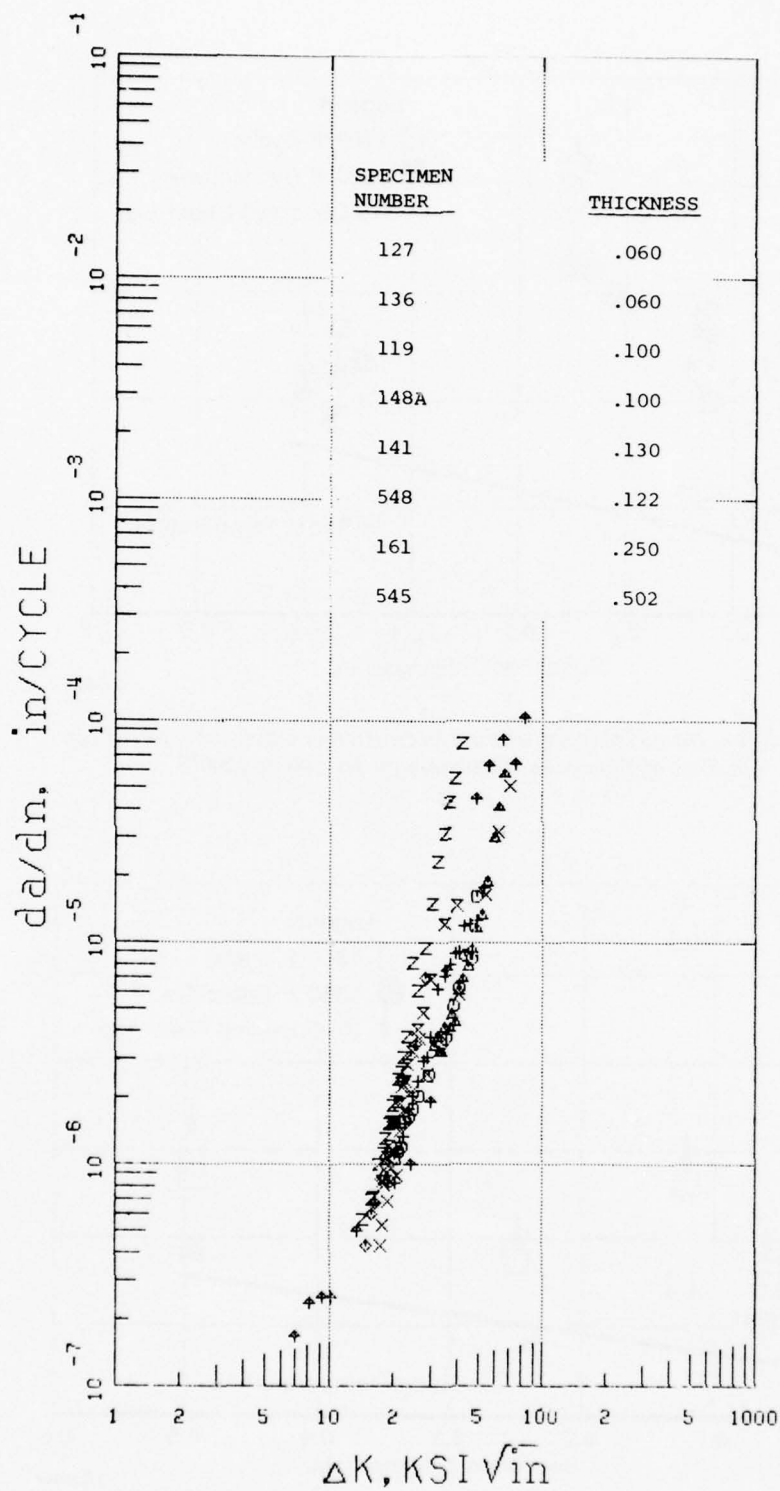
Elevated Temperatures

Figure 6 shows the effect of specimen thickness on the crack propagation rate of IN-100 at 1200°F, 10 cpm, R = 0.1. Specimen thicknesses varied from 0.060 to 0.87-inch. While different geometries and heats were used, it can be concluded that the effect of thickness is minimal (within the bounds of heat-to-heat scatter) at 1200°F, 10 cpm. This result is interesting because, theoretically, the plasticity should be comparable to that at room temperature since the yield strengths are similar. An explanation of this apparent contradiction is provided at the end of this section.

Figure 7 illustrates the effect of specimen thickness on the crack propagation rate of IN-100 at 1200°F, 2-minute dwell, R = 0.1. Within the bounds of heat-to-heat scatter, no difference in crack propagation rate is observed for MCT specimen thicknesses greater than 0.25 inch. It is concluded that minimum section thicknesses of 0.25-inch should be used for mission mix crack propagation tests.

Figures 4 and 5 present the maximum stress intensity at first indication of an observable shear lip (mixed mode) as a function of specimen thickness for IN-100 at room temperature, 1200 and 1350°F. It is noted that mixed mode propagation occurs at lower stress intensities at room temperature than at 1200 or 1350°F for equivalent specimen thicknesses. Furthermore, the 1350°F results (higher oxidation rates) indicated decreased susceptibility to inelasticity effects than at 1200°F. Specimens tested in argon (oxidation minimized) are susceptible to mixed mode propagation at lower maximum stress intensity levels than specimens tested in air.

These results lead to the conclusion that at elevated temperatures, the effect of environmental degradation (oxidation) is to promote crack tip embrittlement, which acts to discourage through-thickness strain. Therefore, plane strain conditions are more possible in an oxidizing atmosphere than in an inert environment.

The sustained load crack propagation characteristics (da/dt, K) for IN-100, at various section thicknesses, at 1200 and 1350°F are presented in figure 8. The qualitative effect of temperature is evident; sustained load crack propagation at 1350°F proceeds more rapidly (by as much as an order of magnitude) than propagation at 1200°F.

8

da/dn, in/CYCLE

ΔK, KSI √in

SPECIMEN NUMBER	THICKNESS
127	.060
136	.060
119	.100
148A	.100
141	.130
548	.122
161	.250
545	.502

SPEC NO	SYMBOL
1000127	O
1000136	△
1000119	+
1000148A	X
1000141	◇
1000548	✦
1000161	⋈
1000545	Z

Figure 3. Room Temperature Thickness Comparison

9
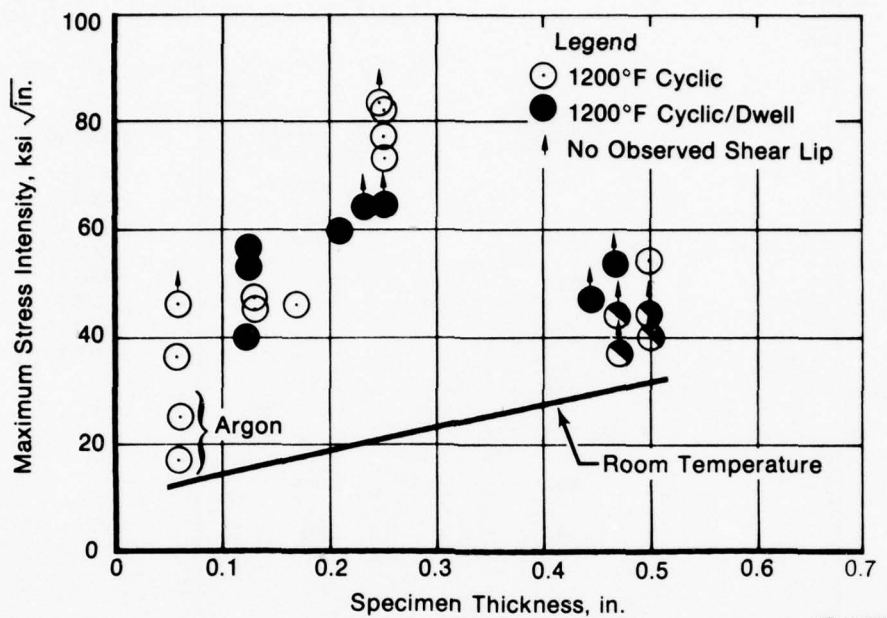
Figure 4. *Maximum Stress Intensity at First Indication of Observable Shear Lip as a Function of Specimen Thickness for IN-100 at 1200°F*
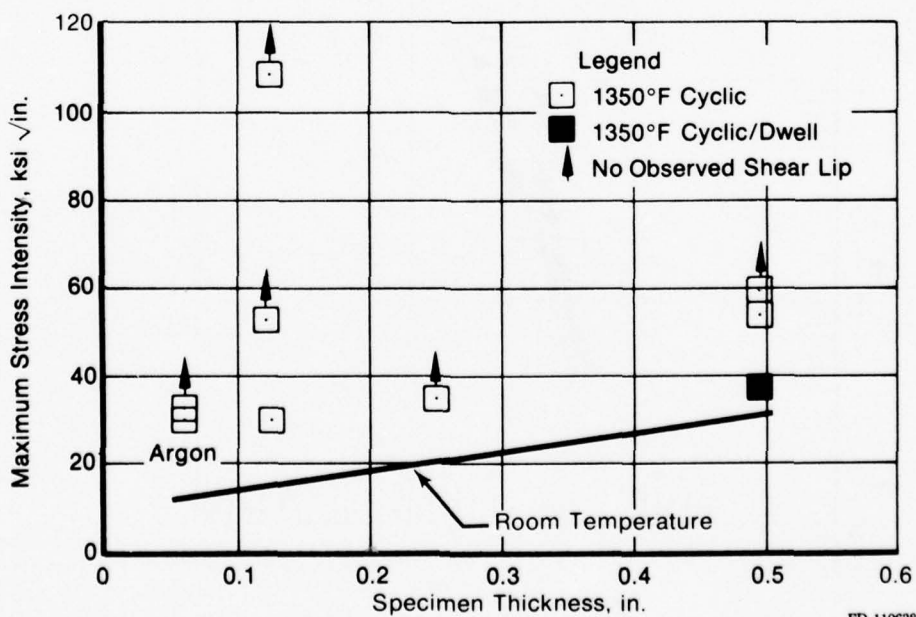
Figure 5. *Maximum Stress Intensity at First Indication of Observable Shear Lip as a Function of Specimen Thickness for IN-100 at 1350°F*

10
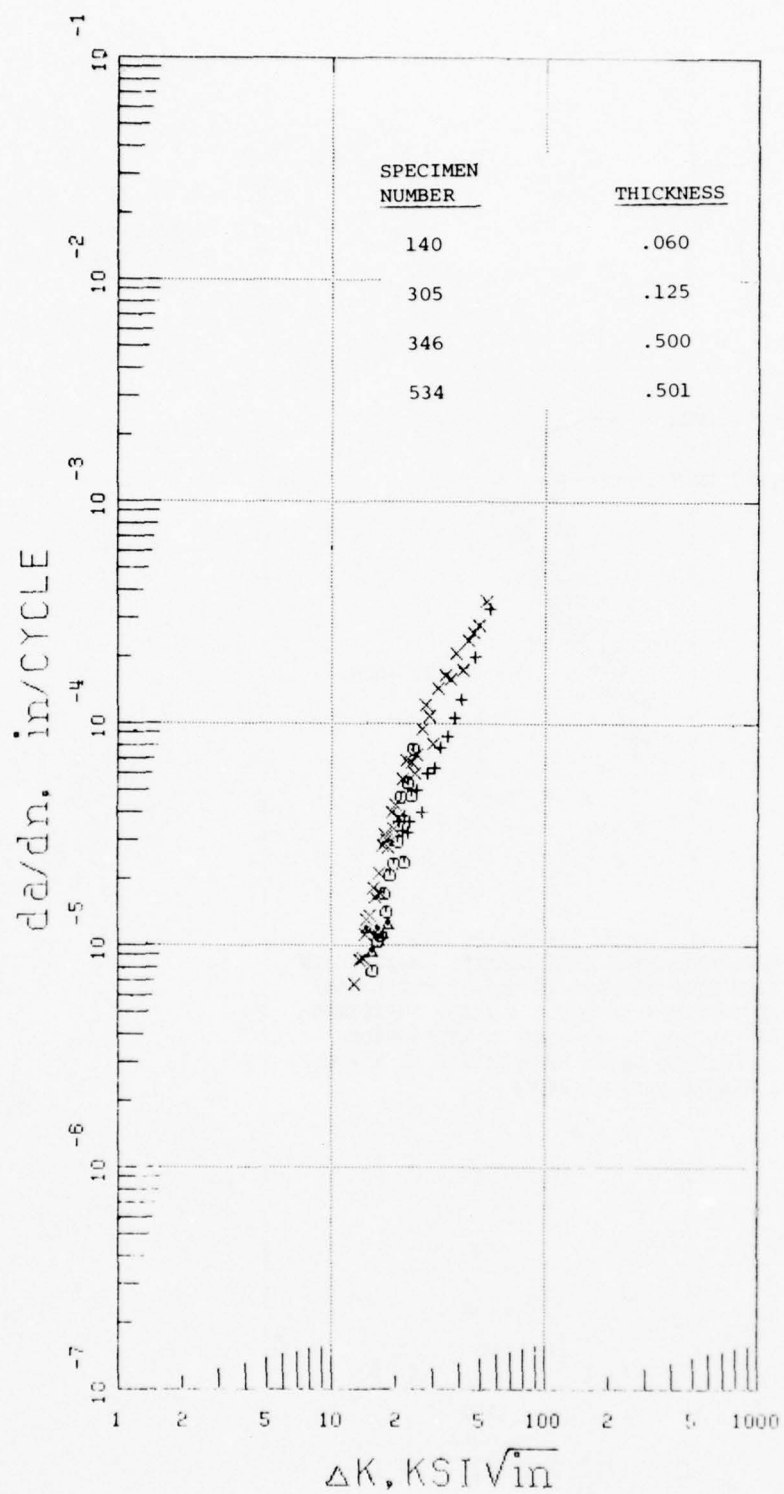
Figure 6. 1200°F Thickness Comparison (10 cpm, R = 0.1)

11
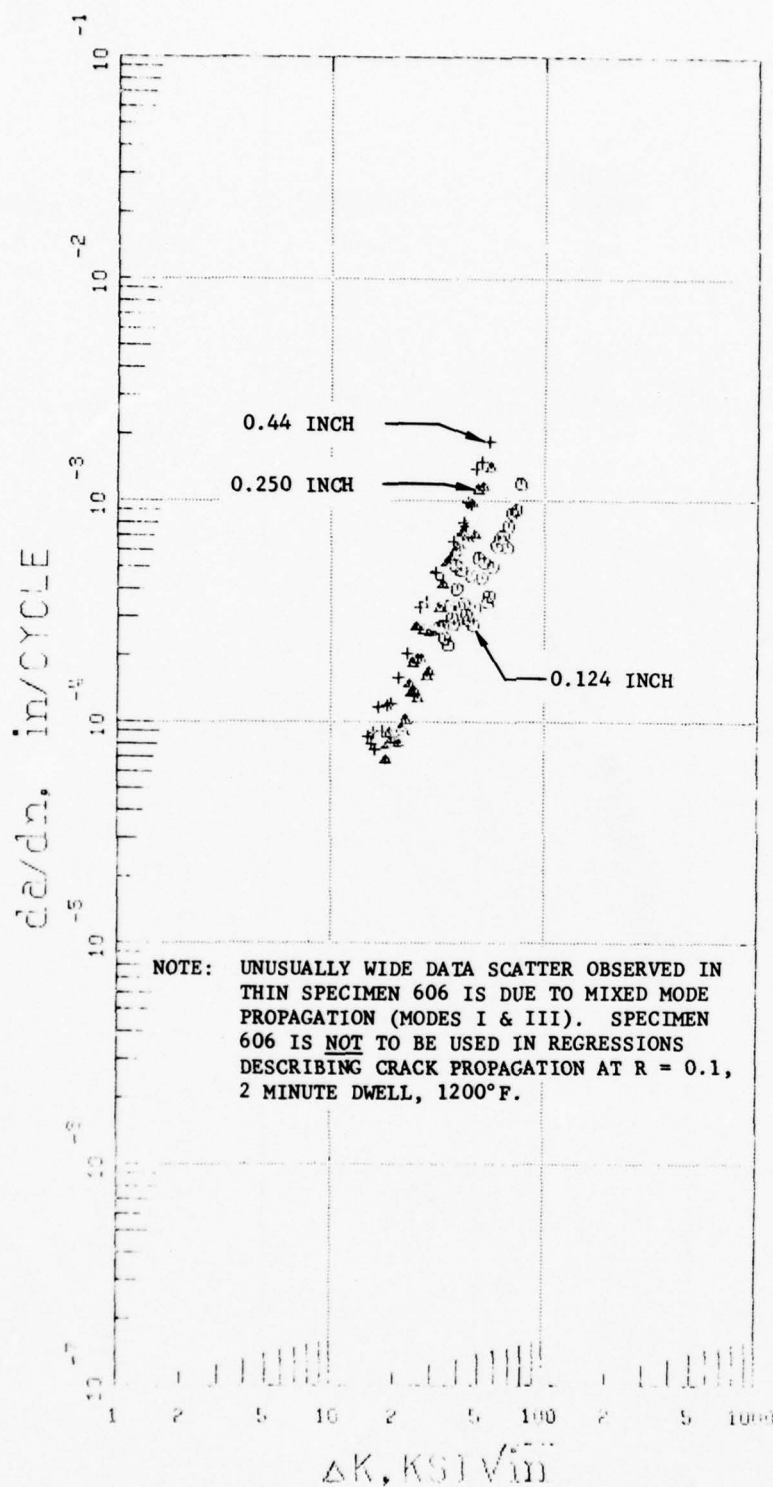
Figure 7. *Effect of Thickness on IN-100 Crack Growth at 1200°F, R = 0.1, 2-Minute Dwell (All MCT Specimens)*

12
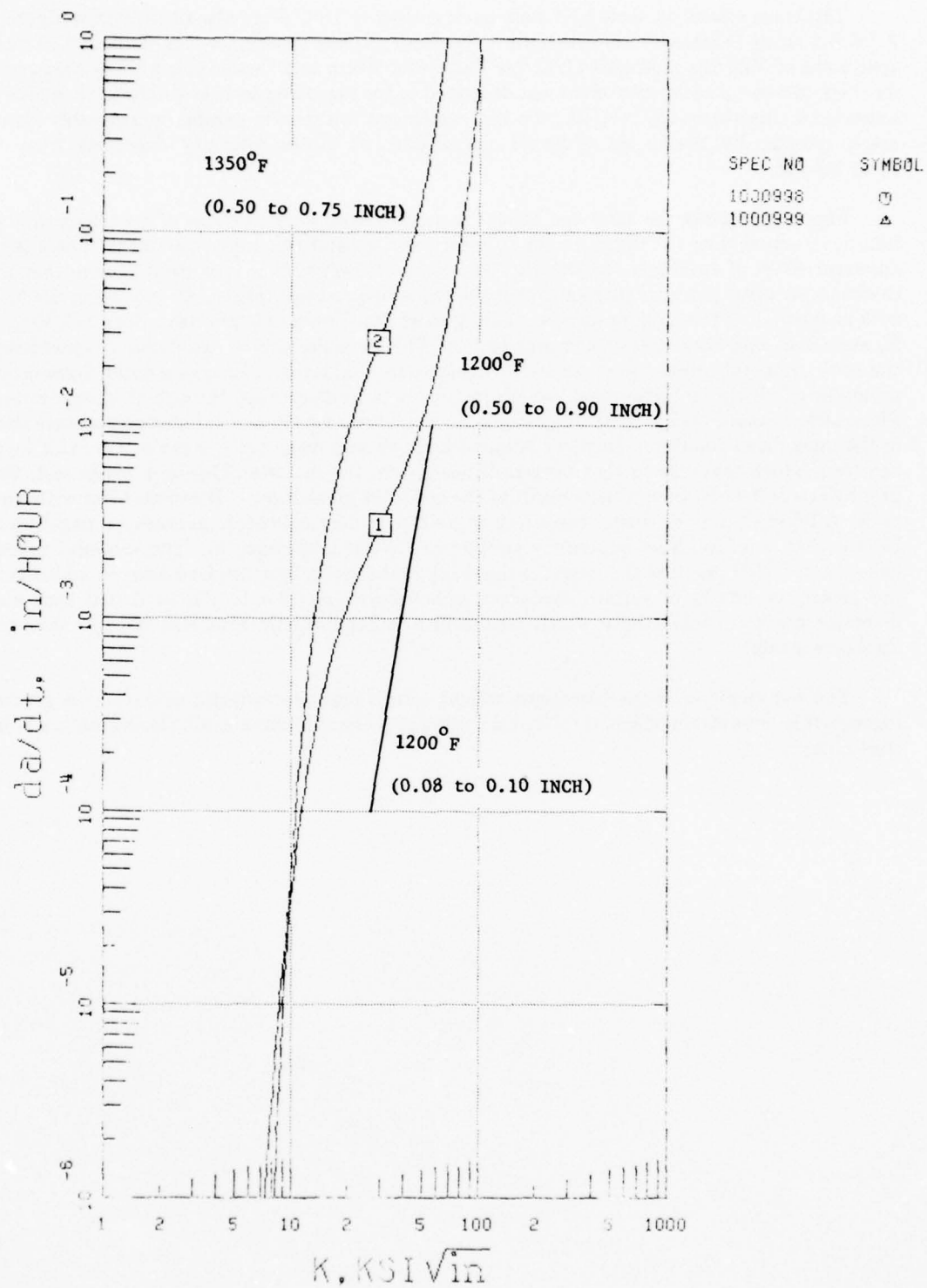
Figure 8. *Effects of Temperature and Specimen Thickness on Sustained Load Crack Propagation Rate*

13

Thickness effects on sustained load crack growth at 1200°F are also illustrated in figure 8. A P&WA study (Reference 12) determined the da/dt, K relationship for thin (0.08 to 0.10 inch) specimens of differing geometries (Double Cantilever Beam and Center Crack). The base curve for thick (0.5 to 0.9-inch) specimens was described in the preceding section and Reference 11. For stress intensities below 50 ksi$\sqrt{\text{in.}}$, the thin specimens are seen to exhibit considerably slower crack growth, by nearly an order of magnitude, as stress intensity decreases from 50 to 30 ksi$\sqrt{\text{in}}$.

Figure 9 presents the 1200 and 1350°F sustained load data in terms of predicted time to failure vs actual time to failure for the 0.50-inch and greater thickness specimens. There is no apparent effect of specimen thickness at 0.5-inch and greater. It is important to note that the thickness required to assure plane strain at the crack tip increases from 0.060-inch for cyclic tests with no dwell, to 0.250-inch for tests containing short time dwells of 5 minutes or less, to 0.50-inch for sustained load subcritical crack propagation. This behavior can be explained by considering the environmental influences on crack tip inelasticity (oxidation). Environmental degradation promotes crack tip embrittlement, which in turn acts to discourage through-thickness strain. Plane strain conditions are therefore possible in thinner sections in an oxidizing atmosphere than in the unoxidized condition. During sustained load, or long dwell tests, a protective oxide layer can form which prevents further oxygen diffusion into the material. During a cyclic test, this prophylactic effect is reduced as a result of the repeated breakdown of the oxide layer with each cycle. A P&WA study describes the effect of grain boundary oxidation on crack propagation in Udimet-700, a nickel-base superalloy similar to IN-100 (Reference 8). The material micro-behavior of U-700 provides the basis for the crack tip behavior hypothesized here. In addition to the protective effects of surface oxidation, enhanced creep, due to the sustained load also increases crack tip inelasticity which results in a larger inelastic zone size (greater through-thickness strain).

The net result of these synergistic effects (creep and prophylactic oxidation) is greater through-thickness strain which necessitates thicker specimens if plane strain constraints are to be maintained.

14

$$T_{calculated} = \int_{a_i}^{a_f} \frac{da}{f(K)}, \quad \text{where:}$$

$$f(K) = da/dt = 10.^{\left\{ C_1 \sinh \left[C_2 (\log (K) + C_3) \right] + C_4 \right\}}$$

and

	1200°F	1350°F
C_1	0.5	0.5
C_2	4.297	5.200
C_3	-1.479	-1.467
C_4	-2.519	-1.570
R^2	0.9975	0.9659
SEE	0.0740	0.1583

Temperature

1200°F □

1350°F △

10^3

10^2

10^1

HOURS TO FAILURE, ACTUAL

10^1 10^2 10^3
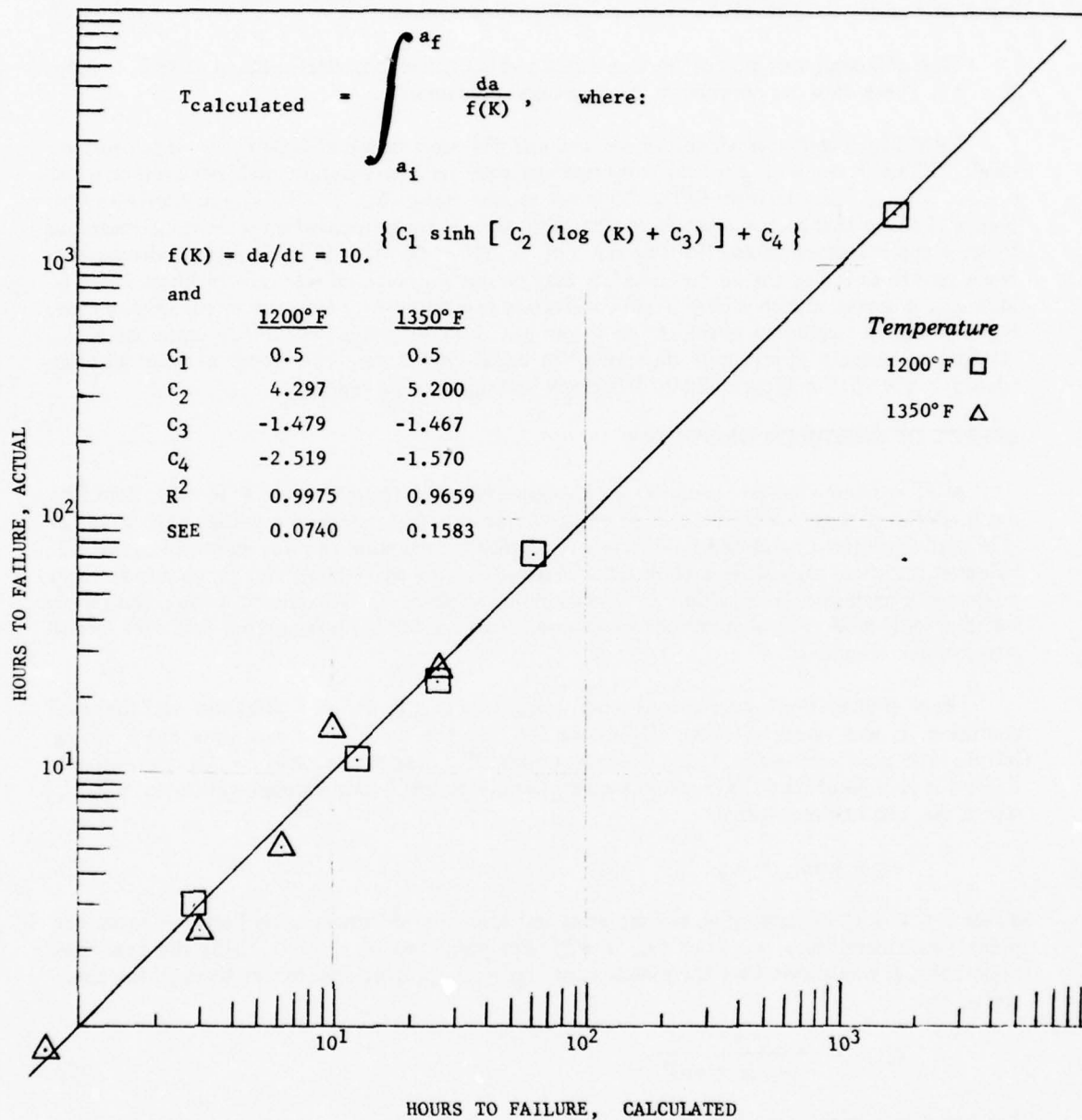
HOURS TO FAILURE, CALCULATED

Figure 9. Actual vs Calculated Times to Failure for 10 MCT Specimens Tested Under Sustained Load at 1200°F and 1350°F

15

EFFECT OF NET SECTION STRESS

The center-crack specimen design was used to determine the effect of stress levels greater than 80% of material yield strength (Reference 4). This specimen was selected because of the small crack size obtainable and the ability to achieve the necessary high net section stresses at stress intensities comparable to existing crack propagation data.

Figure 10 compares high net section stress and low net section stress data at 1200°F, 10 cpm, R = 0.1. These data are observed to be in general agreement.

Eighth-inch center-crack specimens, 649 and 684, were tested at 1200°F, R = 0.1, 2-minute dwell. Different crack length-load combinations were used to produce high net section stress ($\sigma_{net} > 0.8\ \sigma_{yield}$) in specimen 649 and low net section stress ($\sigma_{net} < 0.8\ \sigma_{yield}$) in specimen 684. Figure 11 shows that high σ_{net} produces somewhat slower crack propagation rates at intermediate to high applied stress intensities (40 ksi $\sqrt{in.} \leq \Delta K \leq 60$ ksi $\sqrt{in.}$). This small decrease in crack growth rate, less than a factor of 1.5, may be due to increased through-thickness strain at high σ_{net}, a deviation from plane strain constraints associated with thin specimens. In any case, there is only a negligible effect of using low σ_{net} data to predict cyclic life under high σ_{net} conditions, because appreciable differences in crack growth rate only occur at rates so large (da/dn $> 5 \times 10^{-4}$ inch/cycle) that little crack propagation life remains.

EFFECT OF SPECIMEN GEOMETRY

MCT specimen 606 and center-crack specimen 684 were tested at 1200°F, R = 0.1, 2-minute dwell. Both specimens were 0.125-inch thick. At intermediate stress intensities ($\Delta K < 40$ ksi $\sqrt{in.}$), the specimen exhibited no difference in crack propagation rate (as shown in figure 12). However, at stress intensities greater than 40 ksi $\sqrt{in.}$, the MCT specimen experienced mixed mode crack propagation as evidenced by a pronounced shear lip. This mixed mode propagation was markedly slower, by a factor of two or more, than the Mode I propagation exhibited by the center-crack specimen.

Crack propagation under mixed mode conditions is a function of thickness and material condition. It was recently shown (Reference 13) that the crack tip stress state has a strong influence on plastic zone size. Using the conventional X-Y-Z coordinate axes, where the specimen lies in the X-Y plane, and the crack propagates parallel to the X-axis, through-thickness crack tip stress, σ_{zz}, can be described by

$$\sigma_{zz} = k\ (\sigma_{xx} + \sigma_{yy}) \tag{1}$$

where $0 \leq k \leq \nu^*$ depending on the material and specimen thickness. ν^* is Poisson's ratio. For plane strain conditions, $\sigma_{zz} \geq \nu^*\ (\sigma_{xx} + \sigma_{yy})$. For plane stress, $\sigma_{zz} = 0$. Using the vonMises hypothesis, it was shown that the plastic zone size, r_p, is proportional to this through-thickness stress, or

$$r_p \quad \alpha \quad \frac{K^2}{(\sigma_{yield} + \sigma_{zz})^2} \tag{2}$$

The exact form of this equation analytically predicts a minimum and maximum plastic zone size under plane strain and plane stress conditions respectively. The results of figure 12 suggest that at equivalent stress intensities and thicknesses, σ_{zz} is also a function of geometry.

In section thicknesses that potentially result in mixed mode conditions (0.125-inch in this instance), crack tip stresses can also be a function of specimen geometry. Therefore, it is imperative to test under plane strain conditions to assure universal applicability (in engine disk applications) of the data being generated.

16

da/dn, in/CYCLE

ΔK, KSI √in
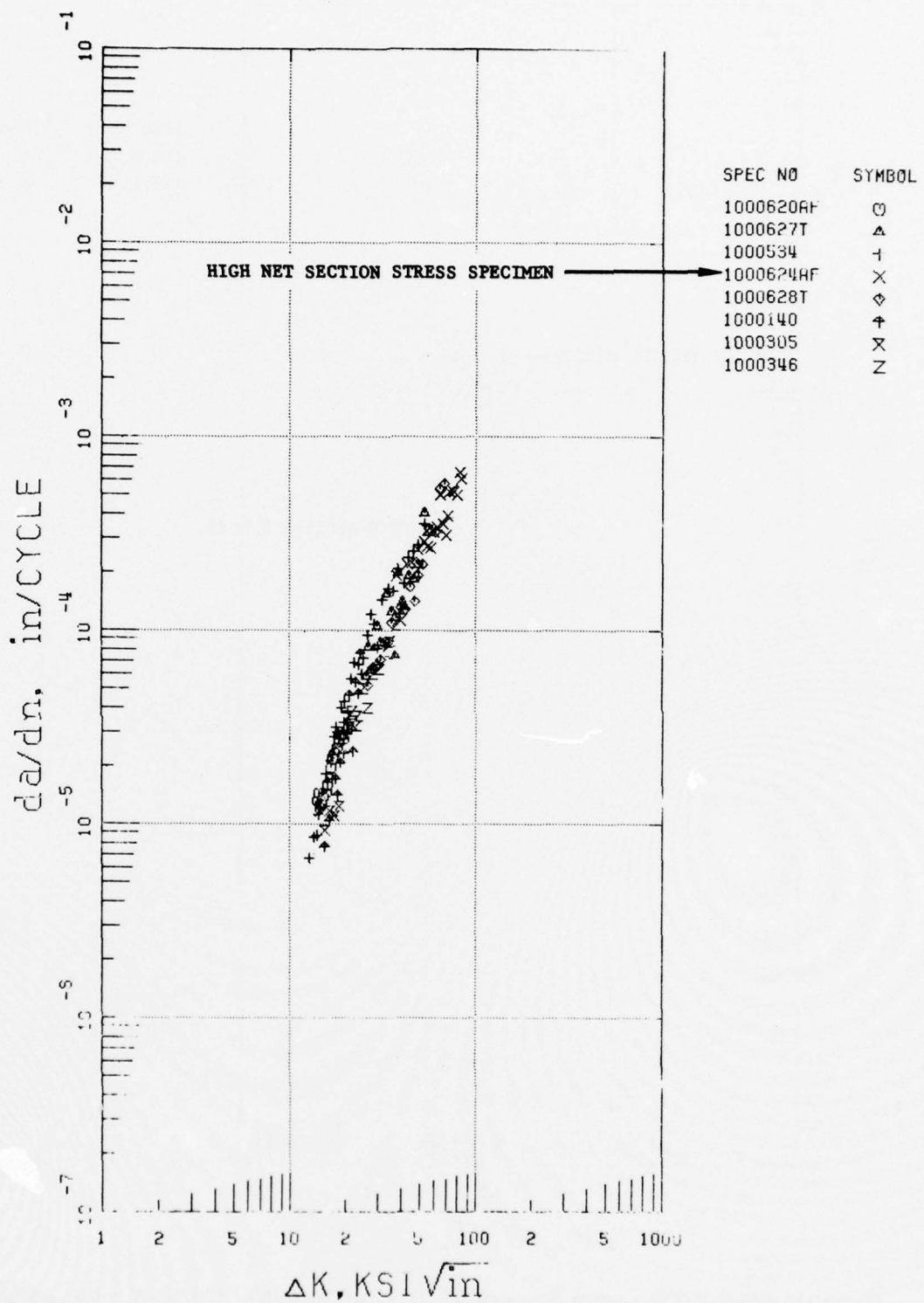
HIGH NET SECTION STRESS SPECIMEN ——————→

Figure 10. Effect of Net Section Stress on IN-100 Crack Growth at 1200°F, R = 0.1, 10 cpm

17
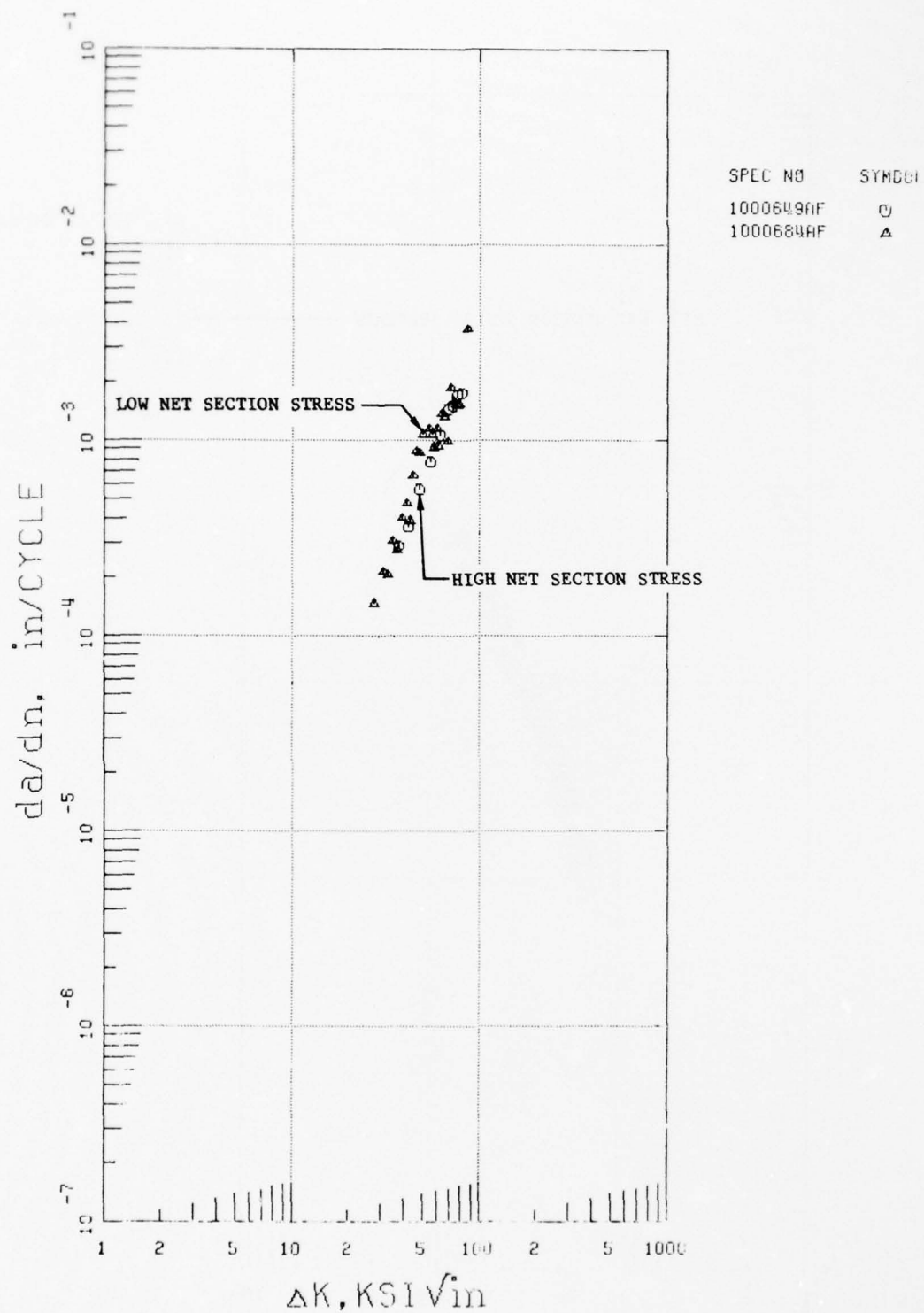
Figure 11. *Effect of Net Section Stress on IN-100 Crack Growth at 1200°F, R = 0.1, 2-Minute Dwell*

18

SPEC NO   SYMBOL

1000606AF   ○

1000684AF   △

CENTER-CRACK
(NO SHEAR LIP)

MODIFIED COMPACT TENSION

GOOD AGREEMENT

MIXED MODE (SHEAR LIP)

NOTE: UNUSUALLY WIDE DATA SCATTER OBSERVED IN
THIN SPECIMEN 606 IS DUE TO MIXED MODE
PROPAGATION (MODES I & III). SPECIMEN
606 IS <u>NOT</u> TO BE USED IN REGRESSIONS
DESCRIBING CRACK PROPAGATION AT R = 0.1,
2 MINUTE DWELL, 1200°F.

da/dn, in/CYCLE

$\Delta K, KSI\sqrt{in}$

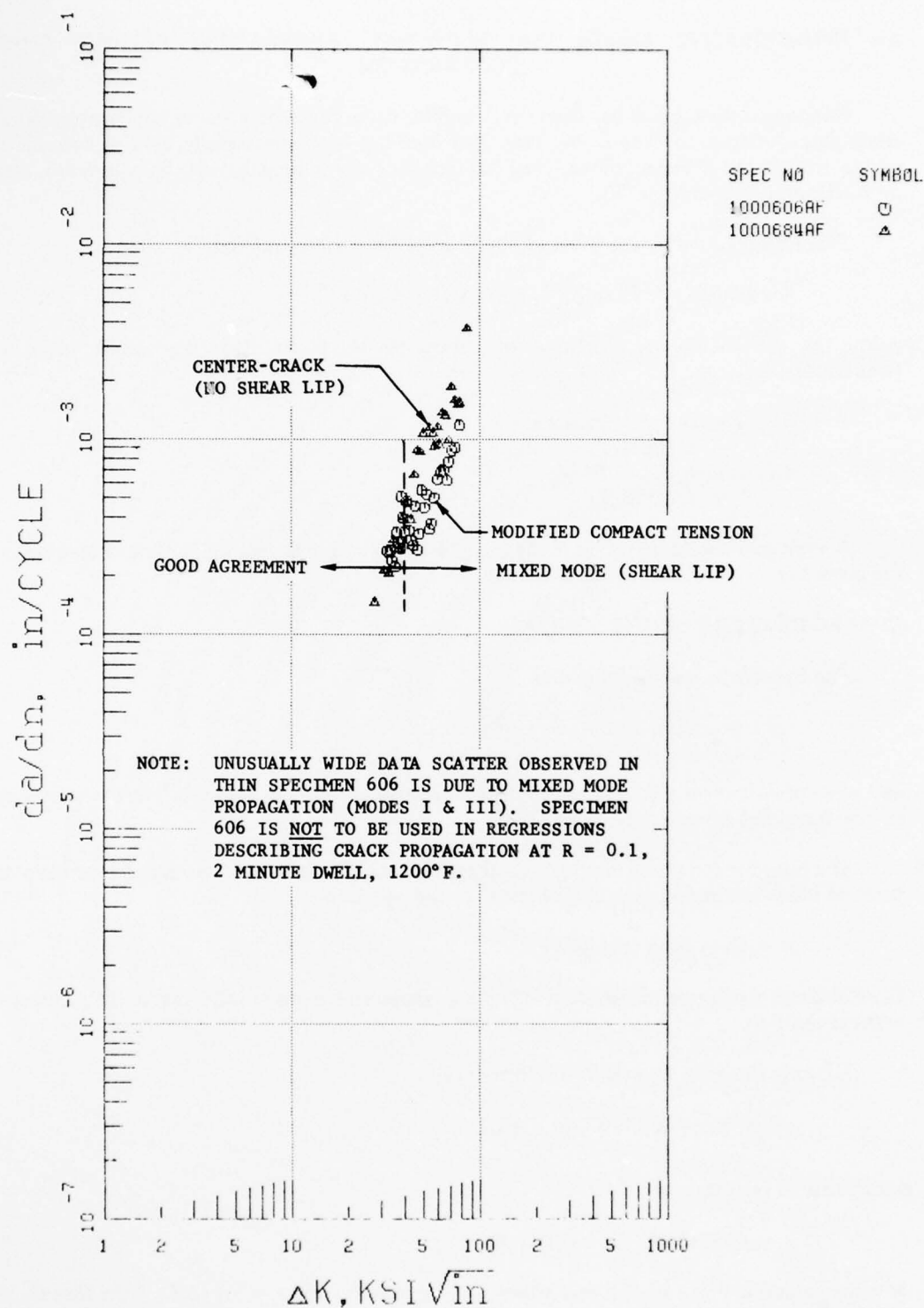*Figure 12. Effect of Specimen Geometry on IN-100 Crack Growth at 1200°F, R = 0.1, 2-Minute Dwell (Thickness = 0.125 inch)*

19

SECTION III
AN INTERPOLATIVE MODEL FOR ELEVATED TEMPERATURE FATIGUE CRACK PROPAGATION

An interpolative model has been developed for the analysis of elevated temperature fatigue crack propagation data. The model presented here has been successfully used to describe the parametric effects of three fundamental influences on crack propagation: frequency (ν), stress ratio (R), and temperature (T).

This interpolative model is based on the hyperbolic sine equation,

$$\log (da/dN) = C_1 \sinh (C_2 (\log (\Delta K) + C_3)) + C_4 \tag{3}$$

where the coefficients are simple empirical functions of test frequency, stress ratio, and temperature:

$$
\begin{aligned}
C_1 &= \text{material constant} \\
C_2 &= f_2 (R, \nu, T) \\
C_3 &= f_3 (C_4, \nu, R) \\
C_4 &= f_4 (\nu, R, T)
\end{aligned}
$$

A more complete description of the model is presented in Reference 14. The salient features are given here.

CHARACTERISTICS OF THE SINH

The hyperbolic sine is defined as

$$y = \sinh x = \frac{e^x - e^{-x}}{2} \tag{4}$$

and when presented on cartesian coordinates it appears as shown in figure 13. The function is zero at $x = 0$ and has its inflection there.

The introduction of the four regression coefficients, C_1 through C_4, permits relocation of the point of inflection and scaling of both axes. In the equation

$$y - C_4 = \sinh (x + C_3) \tag{5}$$

C_3 establishes the horizontal location of the hyperbolic sine point of inflection and C_4 locates its vertical position.

To scale the axes, C_1 and C_2 are introduced

$$\frac{(y - C_4)}{C_1} = \sinh (C_2 (x + C_3)) \tag{6}$$

which can be rewritten as

$$y = C_1 \sinh (C_2 (x + C_3)) + C_4 \tag{7}$$

of which equation 3 is a special case where $y = \log (da/dN)$ and $x = \log (\Delta K)$. Note that C_3 has units of $\log (\Delta K)$ and C_4 has units of $\log (da/dN)$; C_1 and C_2 are dimensionless and can be conceptualized as stretching the curve vertically and horizontally, respectively. Experience indicates that, for a given material, C_1 can be fixed without adversely affecting model flexibility. For IN-100, C_1 has a fixed value of 0.5.

20

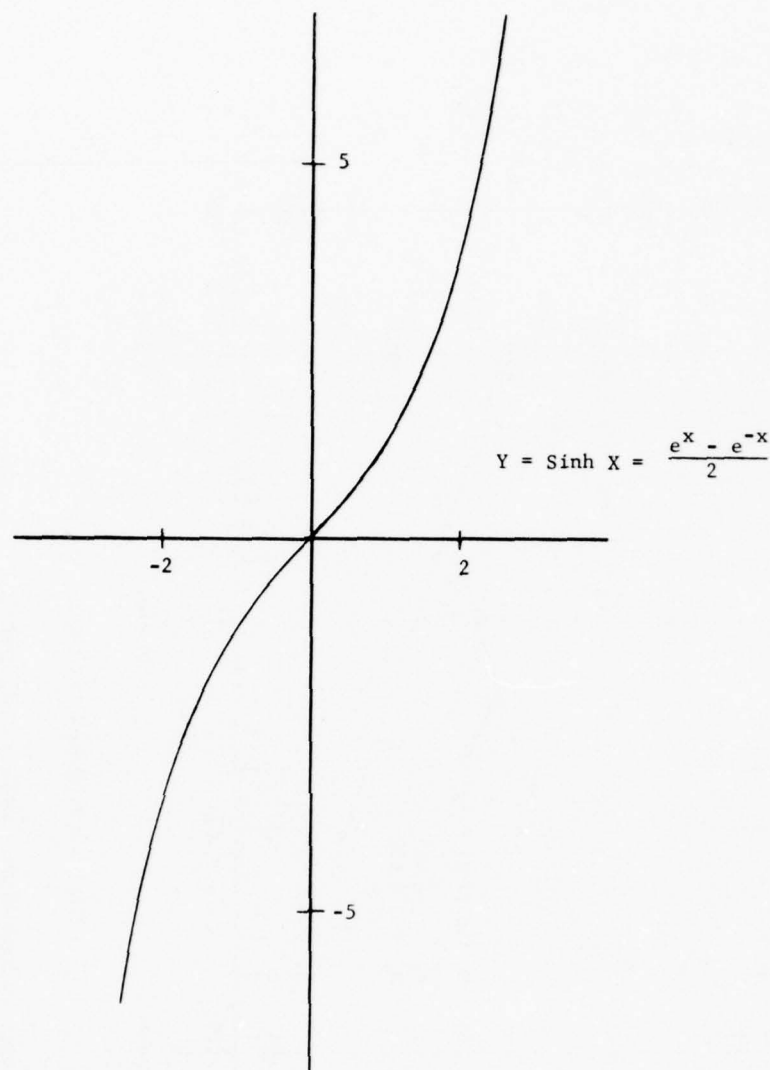$$Y = \text{Sinh } X = \frac{e^x - e^{-x}}{2}$$

Figure 13. Hyperbolic Sine on Cartesian Coordinates

QUANTITATIVE EFFECTS OF CYCLIC FREQUENCY, STRESS RATIO, AND TEMPERATURE

It has been shown that for IN-100, the coefficients in Equation 3 are simple empirical functions of cyclic frequency, stress ratio, and temperature (Reference 14). C_2 and C_4 are logarithmic functions of cycle duration, $1/\nu$ (figure 14). C_3 exhibits linear variation with $\log (1-R)$ as shown in figure 15, where R is the stress ratio. C_2 and C_4 are linear functions of temperature (figure 16), from 1000 to 1350°F, and C_3 does not change because the correlation line is vertical. The relationships for frequency, stress ratio, and temperature are given in figures 17 through 20.
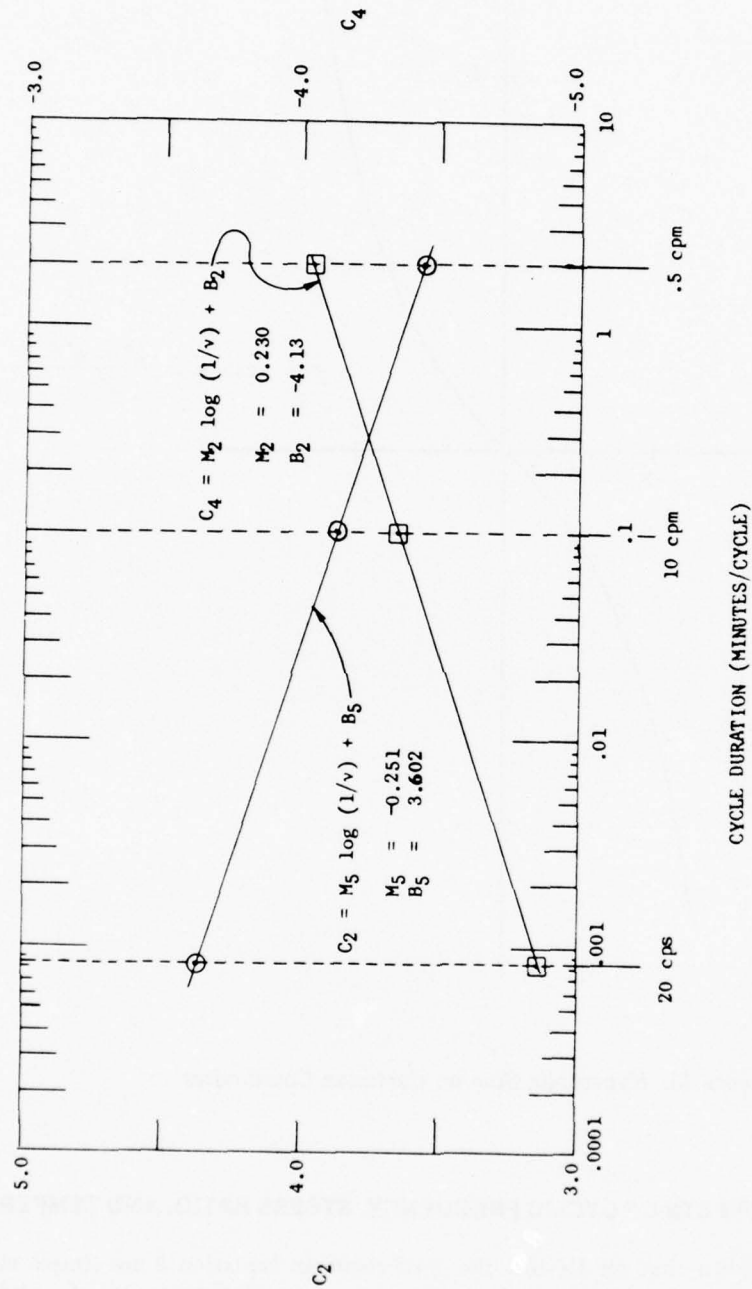
21

Figure 14. *Effect of Frequency on Sinh Model Coefficients C_2 and C_4.*

The figure shows plots with axes C_4 (ranging -3.0, -4.0, -5.0) and C_2 (ranging 5.0, 4.0, 3.0). The horizontal axis is CYCLE DURATION (MINUTES/CYCLE) with markings at $.0001$, $.001$, $.01$, $.1$, 1, 10 and cycle-per references 20 cps, 10 cpm, $.5$ cpm.

$$C_4 = M_2 \log (1/v) + B_2$$
$$M_2 = 0.230$$
$$B_2 = -4.13$$

$$C_2 = M_5 \log (1/v) + B_5$$
$$M_5 = -0.251$$
$$B_5 = 3.602$$

22

R = .8   R = .5   R = .1

$C_3 = M_4 \log (1-R) + B_4$

$M_4 = -0.805$
$B_4 = -1.423$

20 cps

10 cpm

C_3

$C_3 = M_4 \log (1-R) + B_4$

$M_4 = -0.544$
$B_4 = -1.442$

0.1   .5   1.0

1-R
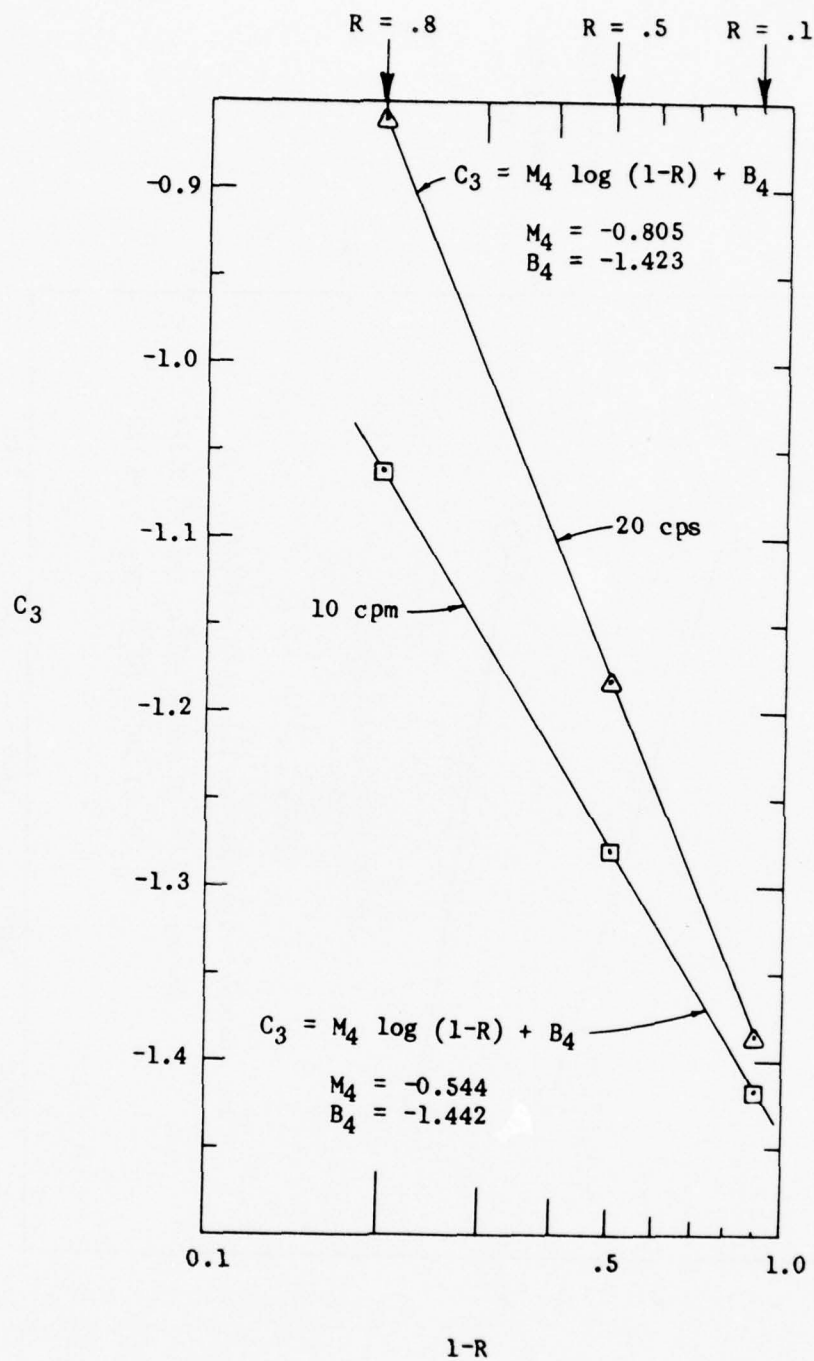
Figure 15. Effect of Stress Ratio, R, on Sinh Model Coefficient, C_3

23

HYPERBOLIC
SINE
COEFFICIENT
c_4

−2.0

−3.0

−4.0

−5.0

c_4

c_2

1400

1300

1200

1100

1000

TEMPERATURE (°F)

IN-100 TEMPERATURE MODEL
10 cpm
R = 0.1
1000°F - 1350°F

$\log (da/dn) = 0.5 \text{ SINH } (C_2 (\log (\Delta K) - 1.417)) + C_4$

where: $C_2 = (2.936 \times 10^{-3}) \; T°_F + 0.377$

$C_4 = (1.557 \times 10^{-3}) \; T°_F - 6.122$

5.0

4.0

3.0

2.0

HYPERBOLIC
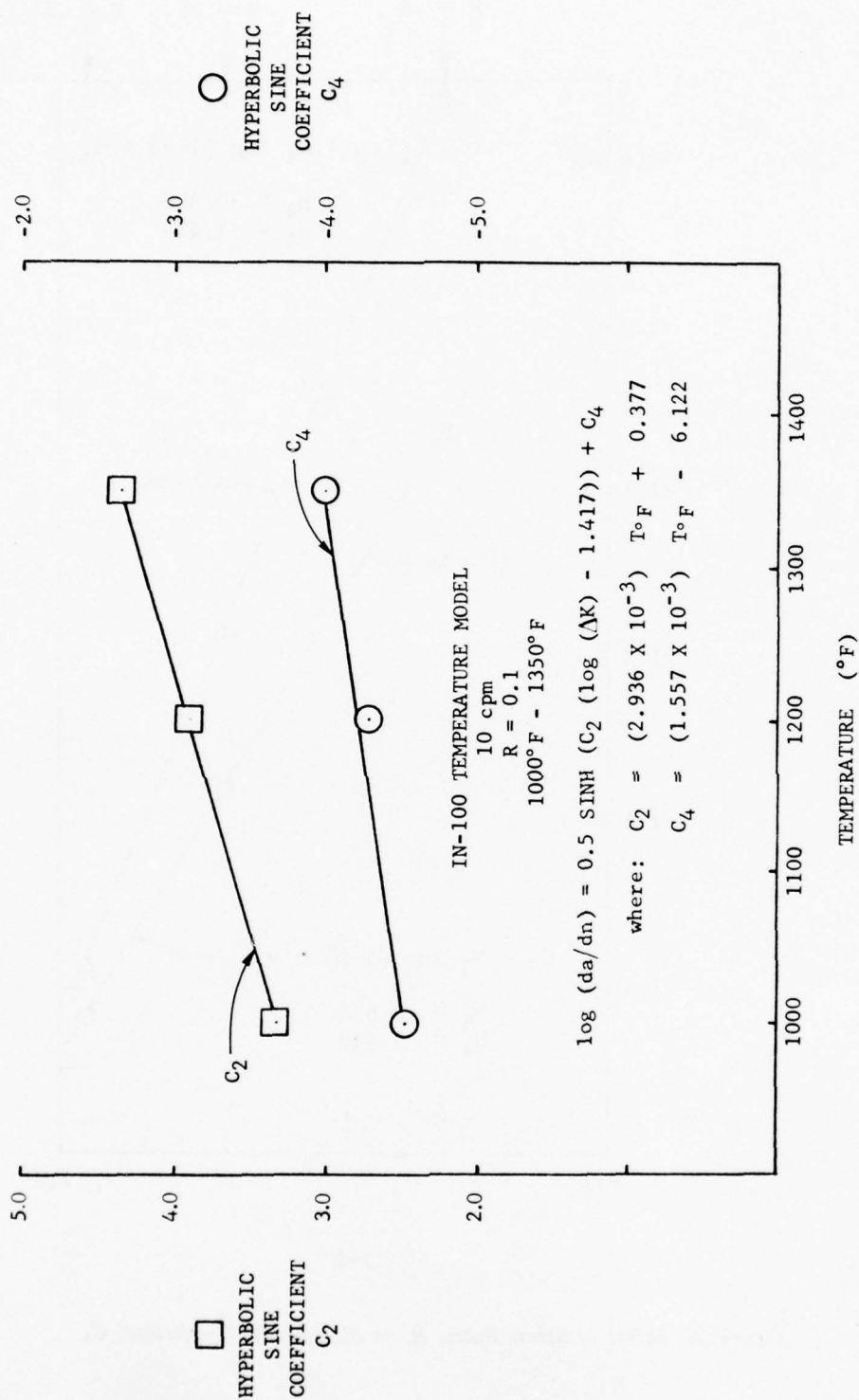SINE
COEFFICIENT
c_2

Figure 16. Effect of Temperature on Hyperbolic Sinh Coefficients C_2 and C_4. (1000°F-1350°F, 10 cpm, R = 0.1)

24
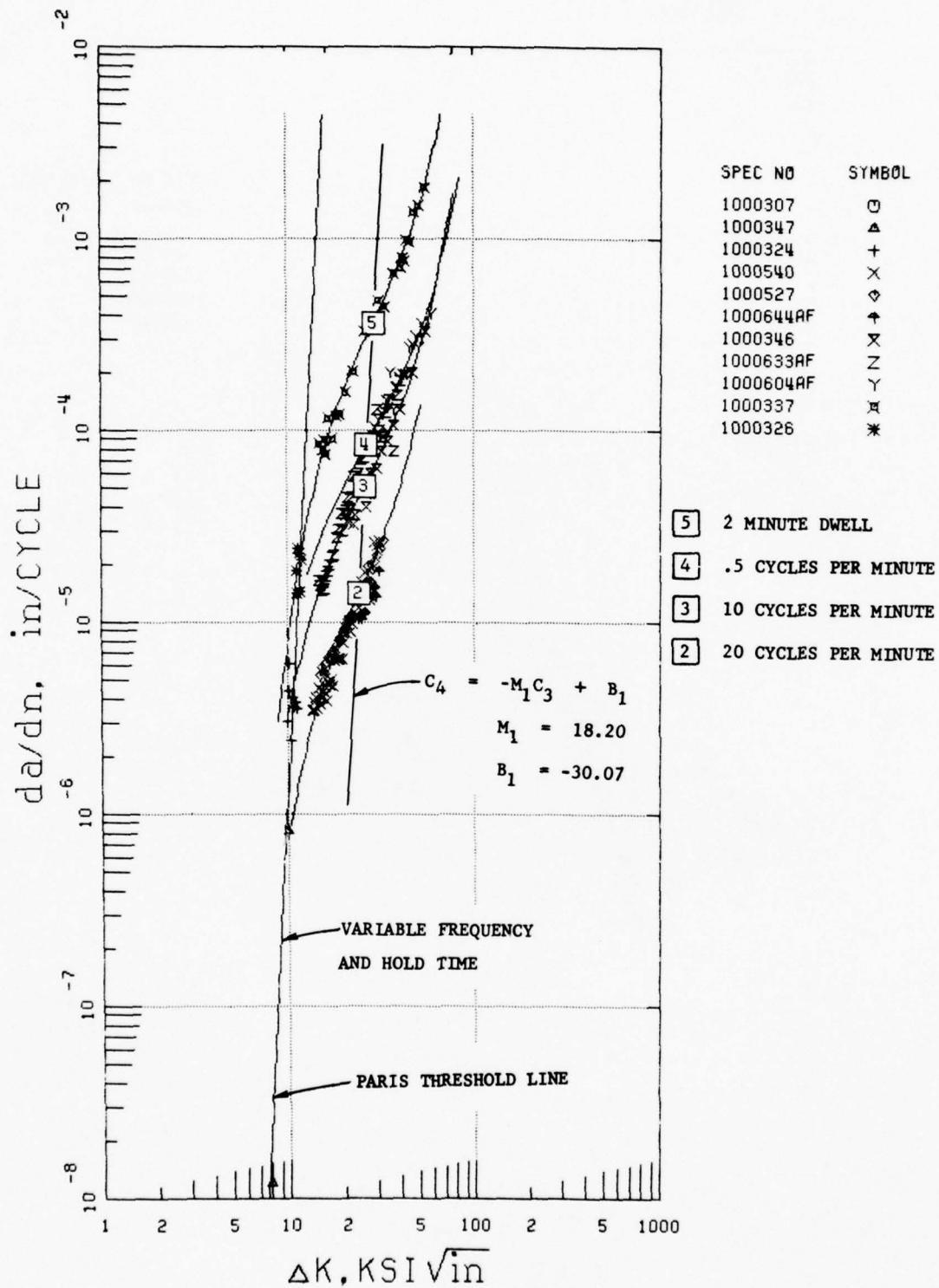
Figure 17. Effect of Frequency on Crack Growth Rate at 1200°F, R = 0.1

25
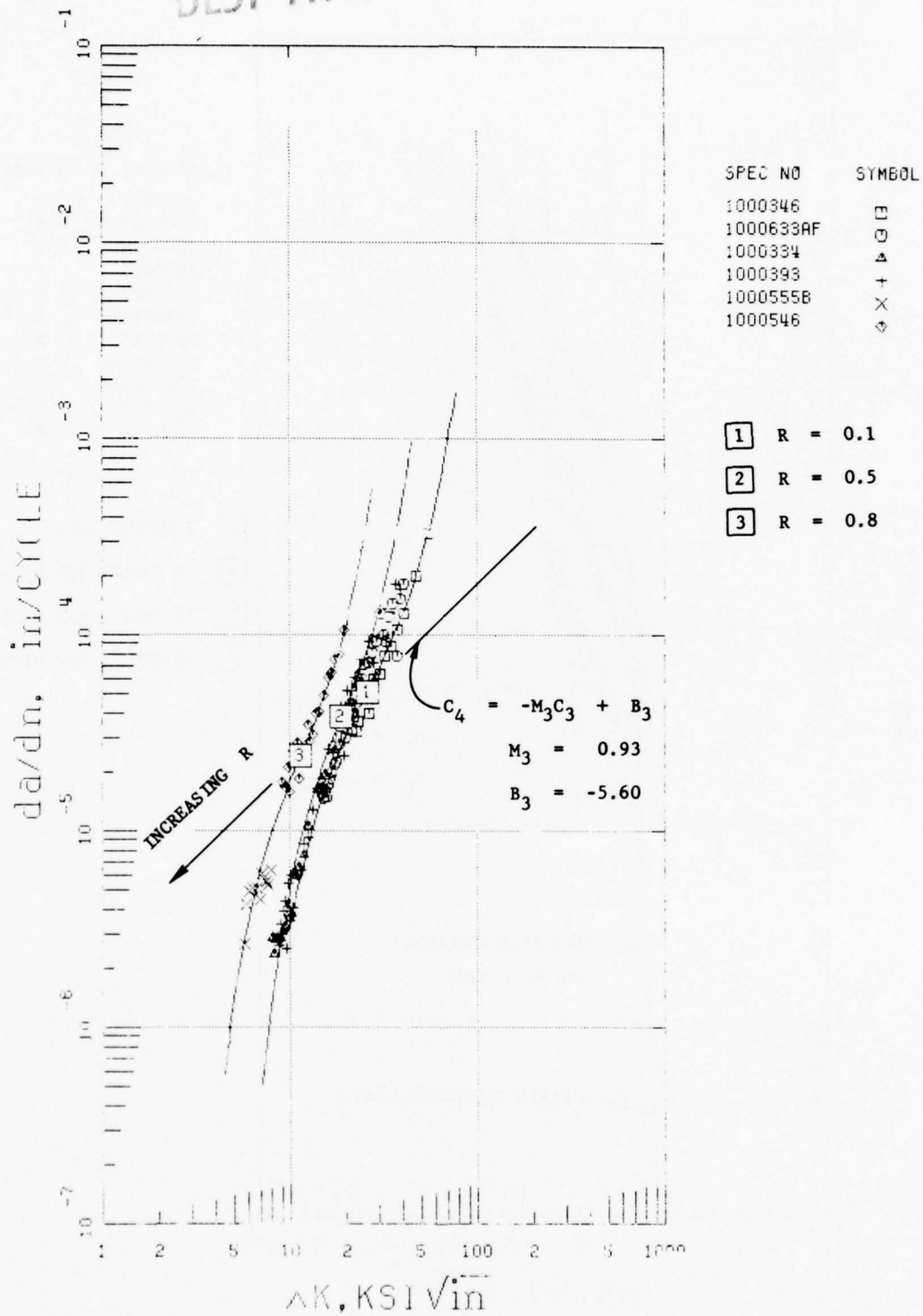
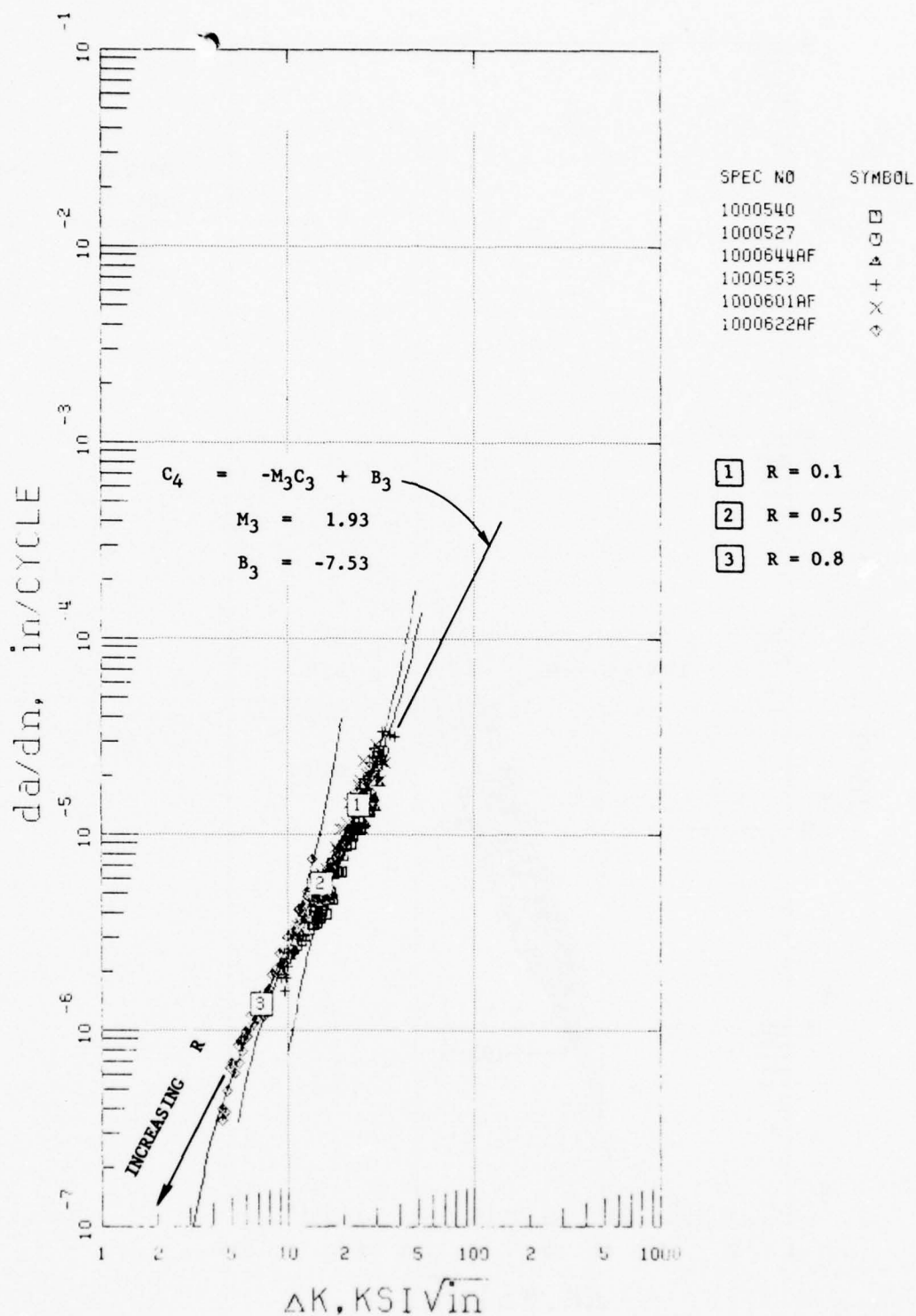Figure 18. *Effect of Stress Ratio on Crack Growth Rate at 1200°F, 10 cpm*

26

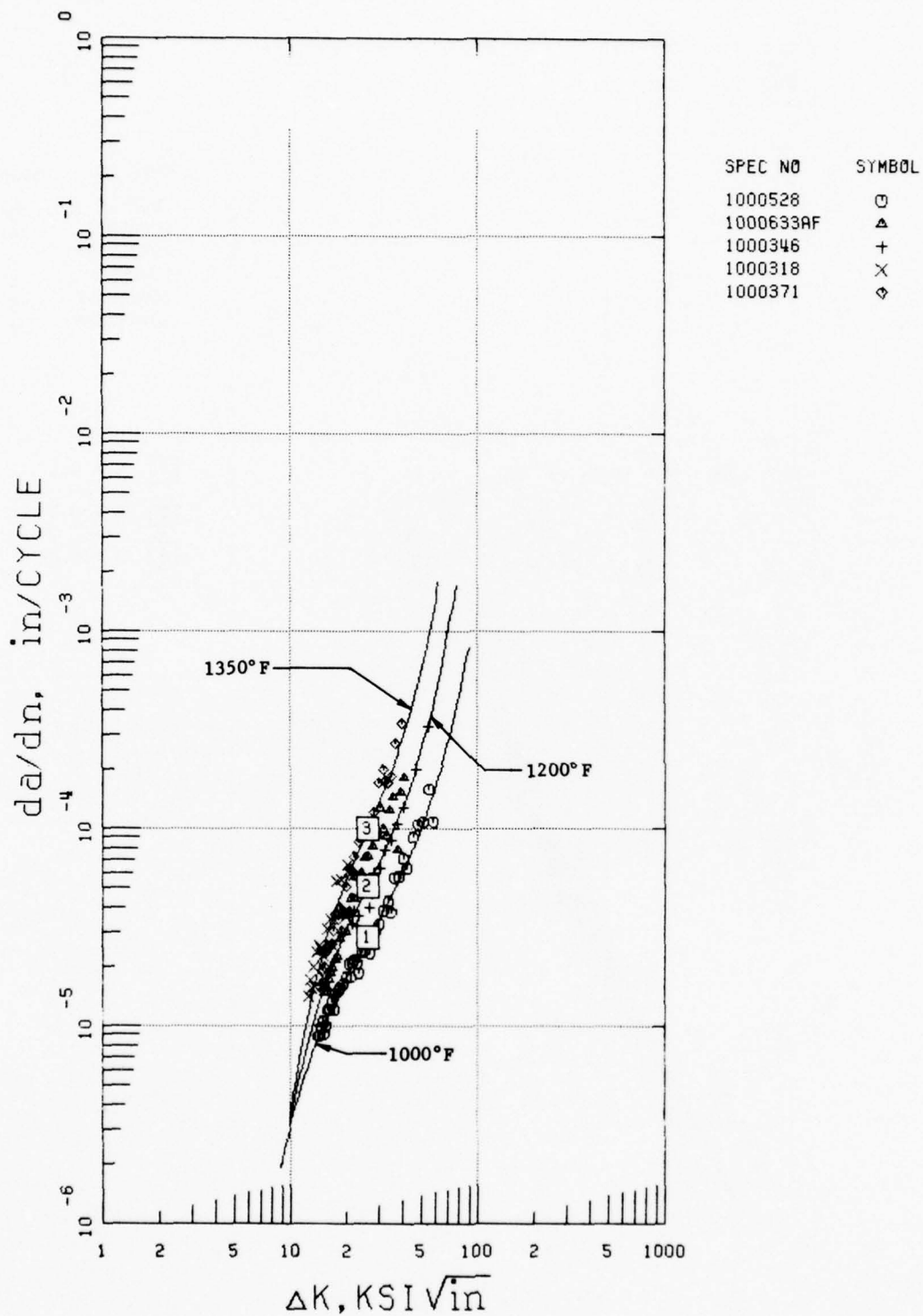Figure 19. *Effect of Stress Ratio on Crack Growth Rate at 1200°F, 20 cps*

27

Figure 20. *Effect of Temperature on Crack Growth Rate at 10 cpm, R = 0.1*

28

USING THE HYPERBOLIC SINE MODEL; INTERPOLATIVE CAPABILITY

The simple relationships discussed previously, describe the propagation behavior of IN-100, in air, at any stress ratio and frequency for temperatures between 1000 and 1350°F. The computational procedure is schematically represented in figure 21: First locate the coefficients on the 1200°F, R = 0.1 frequency model, position 1. Second, account for stress ratio effects by moving along a stress ratio model to position 2. Finally, C_2 and C_4 for the desired temperature are determined using $\partial C/\partial T$ from the temperature model, position 3.
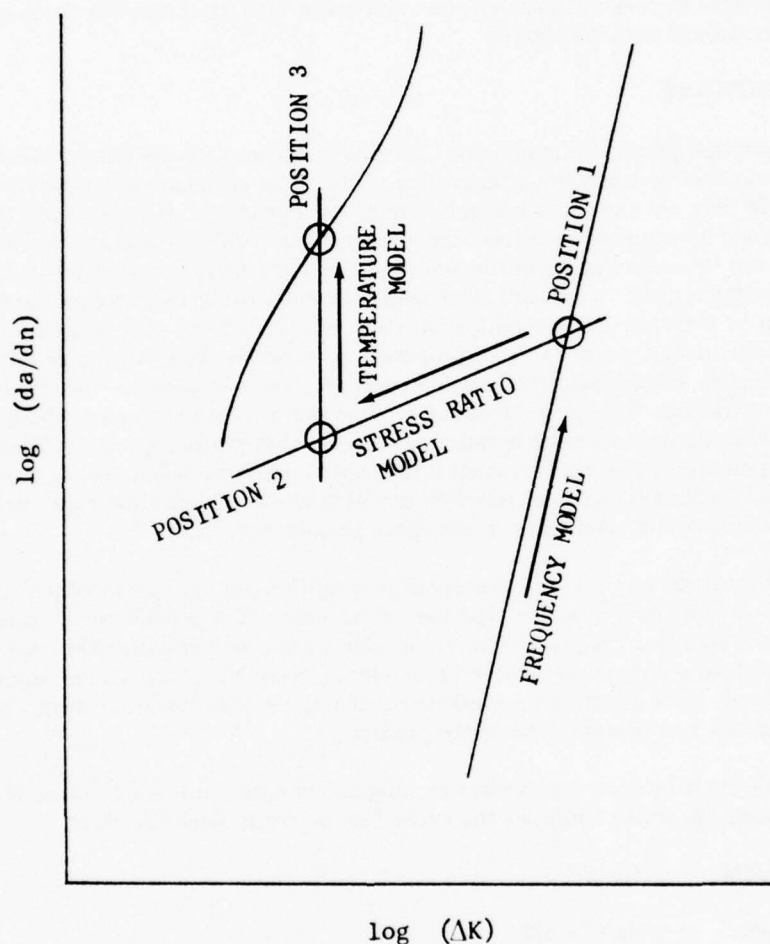

Figure 21. *Schematic Representation of the Method for Determining Sinh Coefficients Representing Any Frequency, Stress Ratio, and Temperature*

29

SECTION IV
SYNERGISTIC EFFECTS OF MISSION VARIABLES

BACKGROUND

The majority of crack growth studies are performed using constant amplitude loading. These tests are not representative of gas turbine rotating component operating conditions, which include complex stress-time-temperature histories. It is expected that crack growth relationships will be complicated by mission mix cyclic conditions that result from throttle excursions, disk-blade interactions, etc.

This section describes synergistic effects of mission variables on IN-100 crack growth. LCF-dwell interactions at constant peak stresses and major load excursion effects on various mission operating conditions are investigated.

LIFE PREDICTIONS

A generalized predictive model must be able to account for the effects of load sequence. A mission should first be analyzed to determine if principles of linear superposition of damage are applicable. If they are not, then synergism must be considered. It is expected that synergistic interactions can be analyzed in at least three ways. First, idealizations (e.g., linear superposition of damage) can be made that result in confident but extremely conservative predictions. This is the least desirable design approach from both cost and engine weight considerations. Second, analyses can be performed to compare synergistic mission effects with predictions based on the quasianalytical models such as those proposed by Wheeler, Willenborg, Elber, Barsom, and Gallagher-Hughes. Generalized predictive models are desirable because their applicability is not limited to operating conditions identical to the test conditions under which a model was developed. Third, empirical models can be developed that predict specific mission effects. This approach is potentially the most accurate if true synergism is modelled, i.e., both retardation and acceleration. It will be shown that the Sinh model is also a vehicle for accurately describing the effects of mission cyclic conditions on the crack growth rates of IN-100.

A mathematical model describing crack propagation has utilitarian value only insofar as it can be used in life prediction and the overall accuracy of a model can be measured by the accuracy of the resulting life prediction. To provide a basis for comparing the accuracy of various predictive models, a simple correlative parameter is used, N_{pred}/N_{act}, the quotient of predicted and actual cyclic lives. Ideally this quotient is 1.0 and decimal deviations from the ideal can be quickly interpreted as percent error of the prediction.

A simple cycle by cycle (or mission by mission) integration is used to sum the incremental crack advances, da, which comprise the cyclic life, N, (or mission life, M).

$$da/dN = f(a, \Delta K \ldots) \tag{8}$$

$$dN = da/f(a, \Delta K \ldots) \tag{9}$$

$$N = \int dN = \int_{a_i}^{a_f} da/f(a, \Delta K \ldots) \tag{10}$$

Because this integral can be difficult to evaluate directly, computerized numerical methods are used.

30

In Equation 8, f (ΔK) is represented by any empirical model that accurately predicts the average instantaneous crack growth rate for a calculated stress intensity. Linear cumulative damage within a mission spectrum is determined using cycle by cycle (or unit time by unit time) integration and subsequent summation of individual components.

$$N_{missions} = \left[\sum_0^{N_c} \frac{da}{f(\Delta K_1)} + \sum_0^{N_d} \frac{da}{f(\Delta K_2)} + \sum_0^{t} \frac{da}{f(K_3)} \right]_{a_i}^{a_f} \quad (11)$$

$$\text{cyclic} \qquad \text{dwell} \qquad \text{sustained} \atop \text{load}$$

Two computer programs have been developed. One, to perform linear superpositon of individual components within a mission mix, and the other to study retardation using quasianalytical models. The first program predicts the life of specimens tested under variable amplitude cyclic, cyclic-dwell, and/or dwell conditions. The mission is segmented and incrementally integrated to predict crack propagation life. The empirical inputs within the mission segments are the interpolative Sinh model coefficients. It is important to note that any of these segments can be a synergistic Sinh model such as those presented later in this section and applied in Reference 15.

The second program performs life analyses for straight cyclic or sustained load crack growth. The Willenborg retardation model (Reference 16) has been incorporated into this program. The applicability of this model for the prediction of crack growth at elevated temperatures has been investigated (Reference 4). Because acceleration as well as retardation has been found to occur, the results of Willenborg model predictions were inconsistent.

Effect of Dwell on IN-100 Crack Growth, 1200°F, R = 0.1

Figure 22 presents a composite plot showing the effect of dwell on the crack growth rate of IN-100 at 1200°F, R = 0.1. It is interesting that there is no appreciable difference between 1-, 2-, and 5-minute dwells. For this reason these data are represented as a single regression. The implication of this observation is that an incubation period exists prior to the onset of sustained load crack propagation, and that this dormant time is due to the exclusion of the pernicious oxidative atmosphere during crack closure. Note that there is a significant difference between the 5- and 10-minute dwells.

Prediction of the dwell specimens lives was made using linear superposition (one cycle at 10 cpm, R = 0.1, 1200°F plus sustained load data at 1200°F).Table 3 shows that these predictions were anticonservative, but the longer the dwell time the more accurate the prediction, thus indicating the observed synergism at the shorter dwell periods.
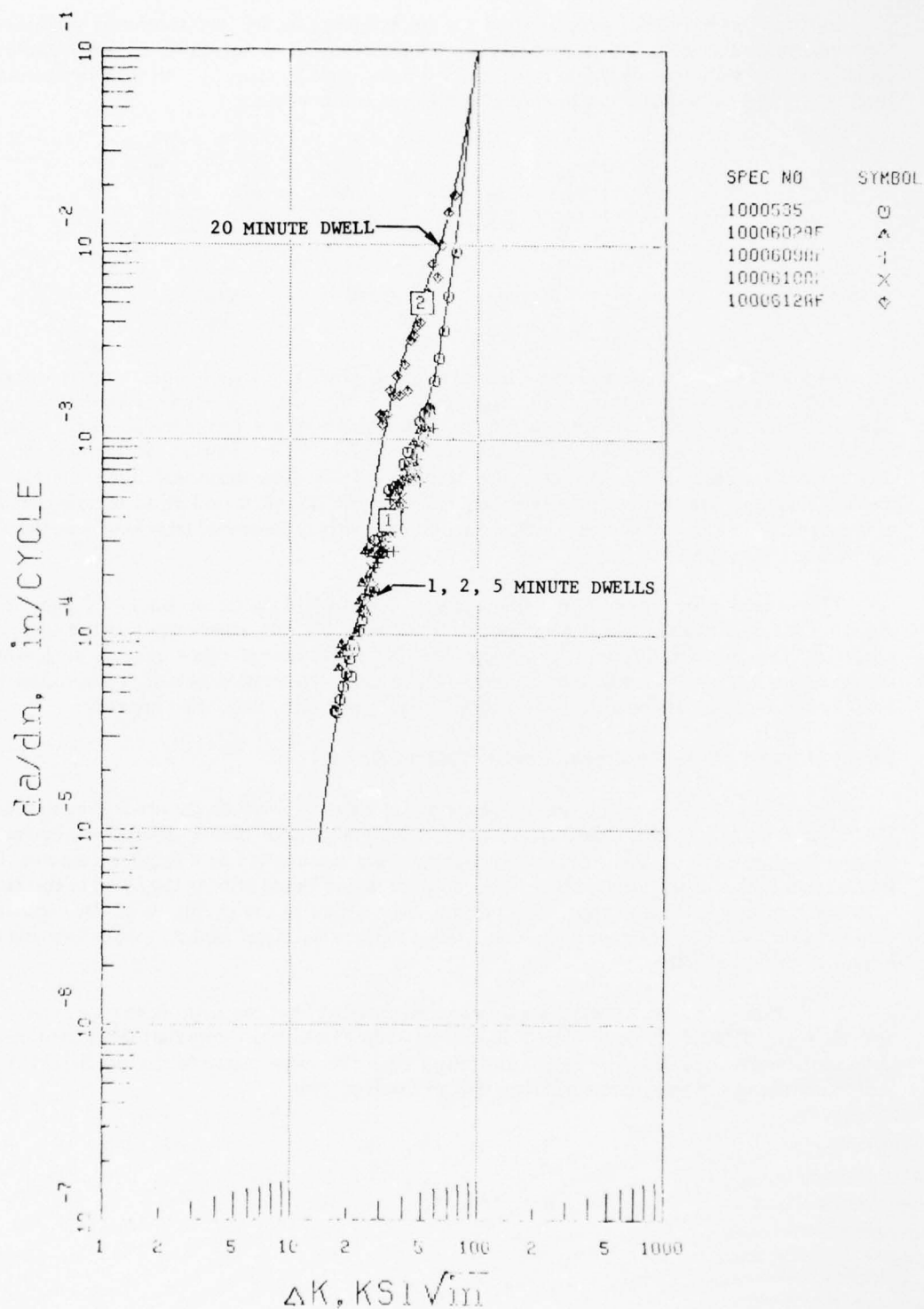
31

Figure 22. *Effect of Dwell on Crack Growth Rate at 1200°F, R = 0.1*

TABLE 3. LCF-DWELL INTERACTION FOR IN-100 AT 1200°F, R = 0.1, LIFE PREDIC-
TION ANALYSIS

Spec. No./Freq.	Initial Crack Size/ Initial Stress Intensity (in./ksi $\sqrt{in.}$)	Final Crack Size/ Final Stress Intensity (in./ksi $\sqrt{in.}$)	Predicted Life	Actual Life	Ratio Predicted/ Actual
535/1 Min. Dwell	1.022/19.0	1.764/56.1	9889	6350	1.557
602/2 Min. Dwell	0.800/20.0	1.676/65.1	7105	4990	1.424
612/20 Min. Dwell	1.051/22.3	1.703/68.2	607	508	1.195

The life predictions are based on superposition of one cycle at 1200°F, 10 cpm, R = 0.1 and sustained load data for 1200°F.

LCF-Dwell Interaction at 1200 and 1350°F

Figures 23 and 24 provide composites of the LCF-dwell interaction crack growth curves at 1200 and 1350°F, respectively. The missions used in these tests are illustrated in Figure 25. Table 4 is a summary of pertinent specimen information and provides a comparison of predicted versus actual lives.

To investigate the effects of combined cyclic and sustained load damage on crack growth in the creep region, specimens were run with combinations of 10/1, 20/1, and 40/1 ratios of cyclic (10 cpm) to 2-minute dwell. Two temperatures were investigated and the laboratory results compared to predicted values on the following basis:

- Using equivalent 10-cpm cycles and predicting total damage with 10 cpm data only.

- Linearly superimposing cyclic damage at 10 cpm and 2-minute dwell damage using cyclic plus 2-minute dwell crack growth data.

- Linearly superimposing cyclic damage and sustained load damage using cyclic plus sustained load crack growth data.

- Considering the mission block data themselves as the basis for predicting residual life.

The comparison assuming equivalent 10 cpm cycles was made to determine if the sustained load damage could be approximated by simple cyclic assumptions. It appears from these limited data that it is justifiable to make this assumption at 1200°F, but not at 1350°F. The results of the predicted vs actual lives are shown in Figures 26 and 27.

The comparison of N_{pred}/N_{actual} for predictions using the mission (da/dM) crack growth data should, and in most cases does, result in the most accurate predictions.

It is encouraging to note the accuracy of predictions using linear superposition of cyclic damage plus sustained load damage. With the exception of specimen 536, all of the cyclic plus sustained load predictions were within 15% of the actual life. These results lend promise to developing degradation models for any dwell time based on sustained load crack propagation data. This model is tested in Reference 15 with encouraging results.
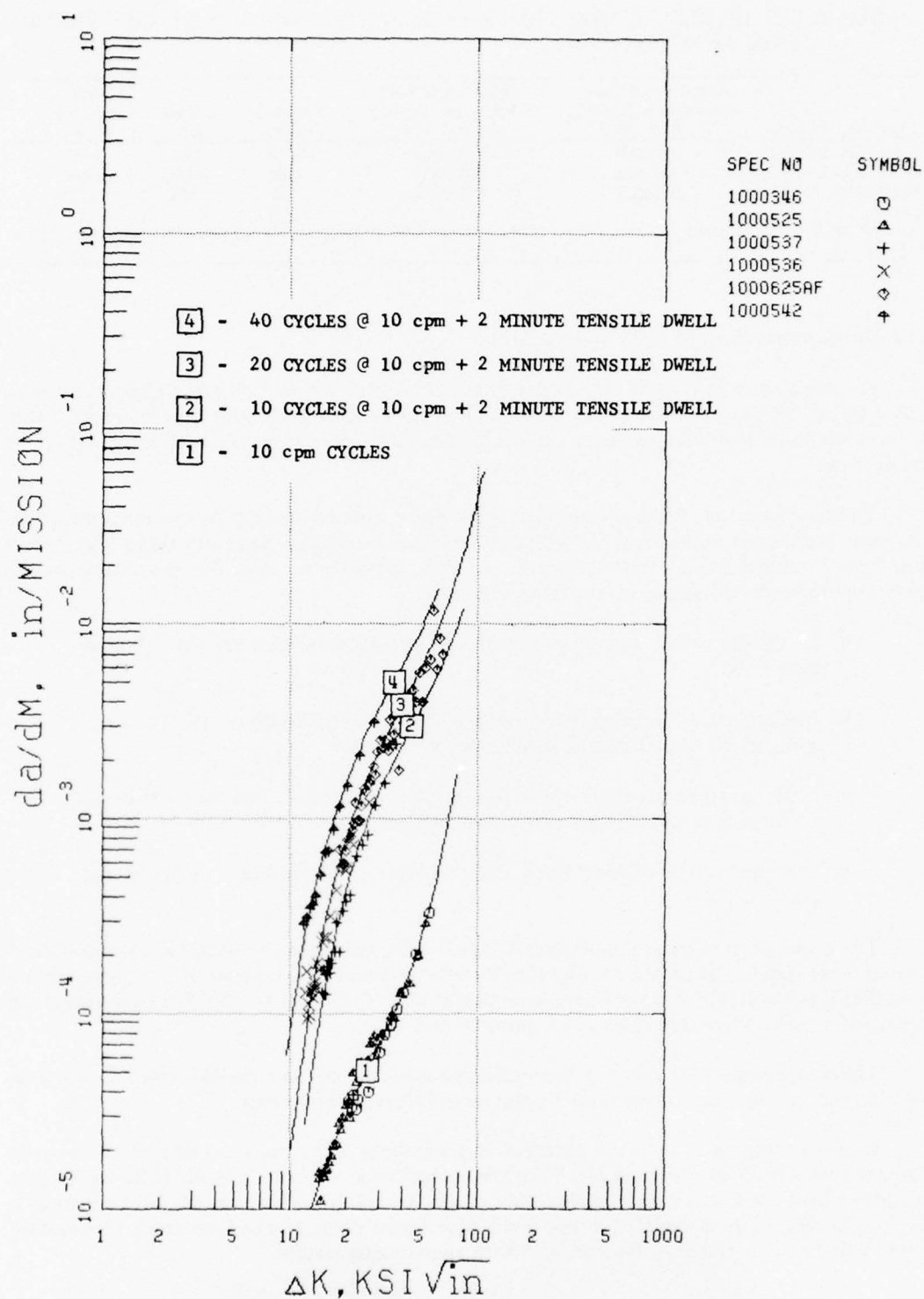
33

SPEC NO   SYMBOL

1000346   ⊕
1000525   △
1000537   +
1000536   ✕
1000625AF   ◇
1000542   ✦

4 — 40 CYCLES @ 10 cpm + 2 MINUTE TENSILE DWELL

3 — 20 CYCLES @ 10 cpm + 2 MINUTE TENSILE DWELL

2 — 10 CYCLES @ 10 cpm + 2 MINUTE TENSILE DWELL

1 — 10 cpm CYCLES

da/dM, in/MISSION

ΔK, KSI√in

Figure 23. LCF-Dwell Interaction, 1200°F, R = 0.1

34
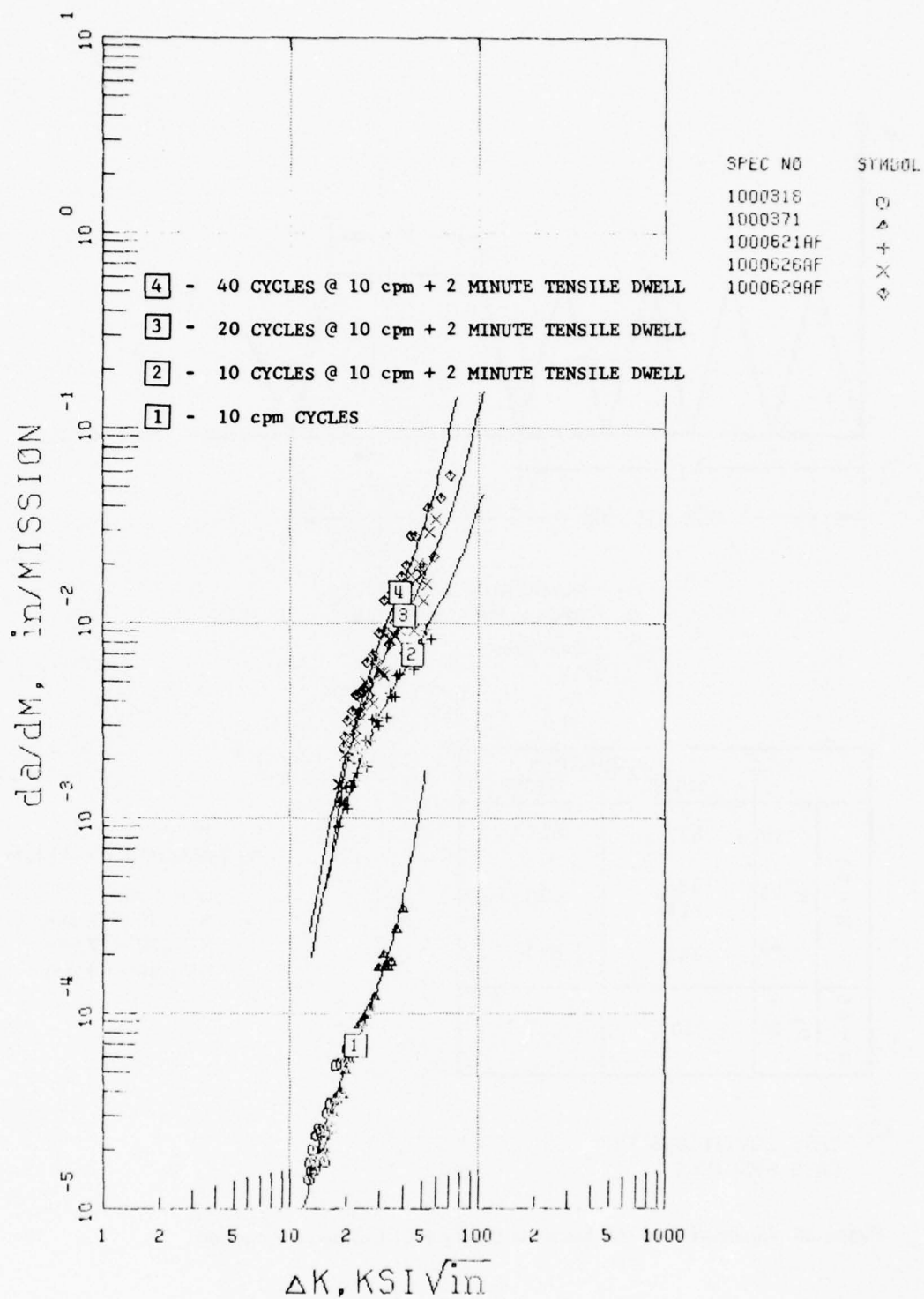
Figure 24. *LCF-Dwell Interaction, 1350°F, R = 0.1*

35
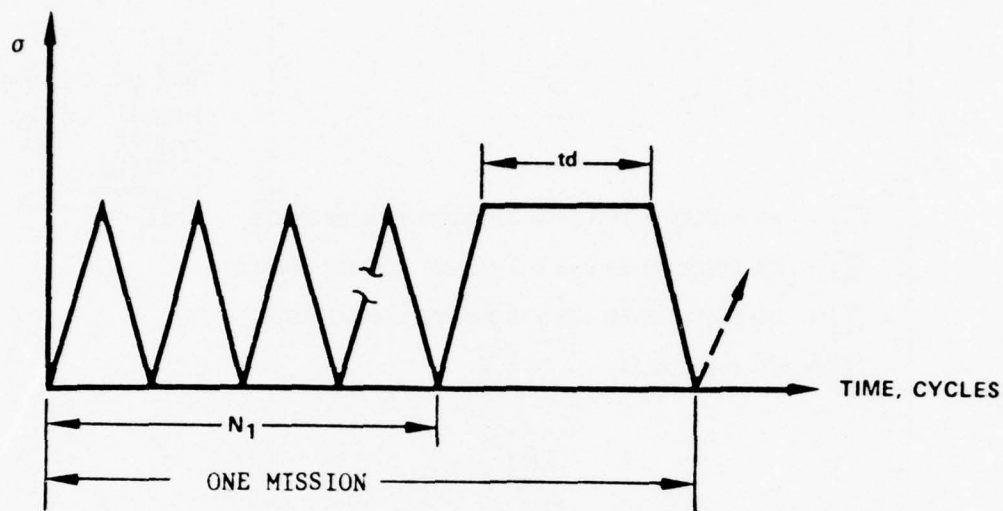
N$_1$ = NUMBER OF LCF CYCLES
td = DWELL TIME, MINUTES
R = $\sigma_{min}/\sigma_{max}$

| | | TEMPERATURE | |
		1200°F	1350°F
R = 0.1	N$_1$ 10	537	621
	N$_1$ 20	536 625	626
	N$_1$ 40	542	629
R = 0.5	N$_1$ 20	630	631

N$_1$ FREQUENCY = 10 cpm

td = 2 min
N$_1$ = 10 = 1 min
N$_1$ = 20 = 2 min
N$_1$ = 40 = 4 min

TEST CONDITIONS FOR
EACH SPECIMEN

Figure 25. Illustration of the Missions Used for LCF-Dwell Interaction

TABLE 4. LCF-DWELL INTERACTION FOR IN-100 AT R = 0.1, LIFE PREDICTION ANALYSIS

(Spec. No.) Analysis Method	Initial Crack Size/ Initial Stress Intensity (in./ksi√in.)	Final Crack Size/ Final Stress Intensity (in./ksi √in.)	Predicted Life	Actual Life	Ratio Predicted/ Actual
(536)					
10 cpm	1.124/13.3	1.735/33.0	1608	2187	0.735
10 cpm + 2 min dwell	1.124/13.3	1.735/33.0	1389	2187	0.635
Mission Mix	1.124/13.3	1.735/33.0	2177	2187	0.995
10 cpm + Sustained Load	1.124/13.3	1.735/33.0	1557	2187	0.712
(537)					
10 cpm	1.089/15.8	1.771/43.6	2025	1925	1.052
10 cpm + 2 min dwell	1.089/15.8	1.771/43.6	1490	1925	0.774
Mission Mix	1.089/15.8	1.771/43.6	2061	1925	1.071
10 cpm + Sustained Load	1.089/15.8	1.771/43.6	1871	1925	0.972
(542)					
10 cpm	1.090/13.0	1.738/33.8	918	931	0.986
10 cpm + 2 min dwell	1.090/13.0	1.738/33.8	853	931	0.916
Mission Mix	1.090/13.0	1.738/33.8	937	931	1.006
10 cpm + Sustained Load	1.090/13.0	1.738/33.8	902	931	0.969
(625)					
10 cpm	0.935/20.4	1.756/63.9	686	561	1.223
10 cpm + 2 min dwell	0.935/20.4	1.756/63.9	566	561	1.009
Mission Mix	0.935/20.4	1.756/63.9	510	561	0.909
10 cpm + Sustained Load	0.935/20.4	1.756/63.9	645	561	1.150
(621)					
10 cpm	0.948/20.0	1.749/60.9	701	339	2.068
10 cpm + 2 min dwell	0.948/20.0	1.749/60.9	426	339	1.257
Mission Mix	0.948/20.0	1.749/60.9	338	339	0.997
10 cpm + Sustained Load	0.948/20.0	1.749/60.9	335	339	0.988
(626)					
10 cpm	0.877/19.7	1.741/68.4	381	218	1.748
10 cpm + 2 min dwell	0.877/19.7	1.741/68.4	285	218	1.307
Mission Mix	0.877/19.7	1.741/68.4	226	218	1.037
10 cpm + Sustained Load	0.877/19.7	1.741/68.4	243	218	1.115
(629)					
10 cpm	0.797/18.8	1.662/84.3	155	122	1.270
10 cpm + 2 min dwell	0.797/18.8	1.662/84.3	133	122	1.090
Mission Mix	0.797/18.8	1.662/84.3	119	122	0.975
10 cpm + Sustained Load	0.797/18.8	1.662/84.3	120	122	0.981

Note:

Specimen 536: One mission = 20 cycles at 10 cpm plus one tensile dwell for 2 minutes at 1200°F
Specimen 537: One mission = 10 cycles at 10 cpm plus one tensile dwell for 2 minutes at 1200°F
Specimen 542: One mission = 40 cycles at 10 cpm plus one tensile dwell for 2 minutes at 1200°F
Specimen 625: One mission = 20 cycles at 10 cpm plus one tensile dwell for 2 minutes at 1200°F
Specimen 621: One mission = 10 cycles at 10 cpm plus one tensile dwell for 2 minutes at 1350°F
Specimen 626: One mission = 20 cycles at 10 cpm plus one tensile dwell for 2 minutes at 1350°F
Specimen 629: One mission = 40 cycles at 10 cpm plus one tensile dwell for 2 minutes at 1350°F
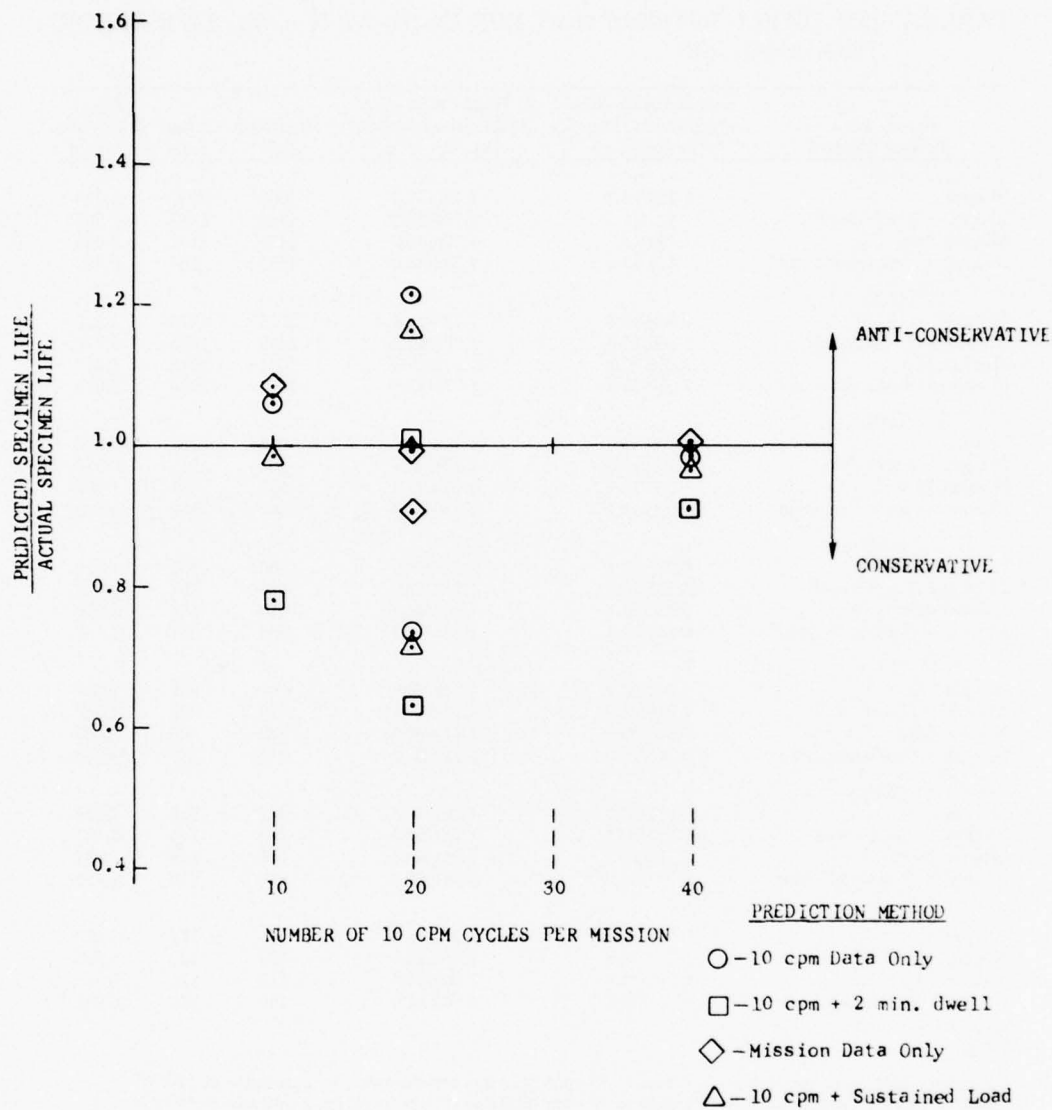
Figure 26. *Life Predictions for LCF-Dwell Interaction Test Specimens for IN-100, 1200°F,*
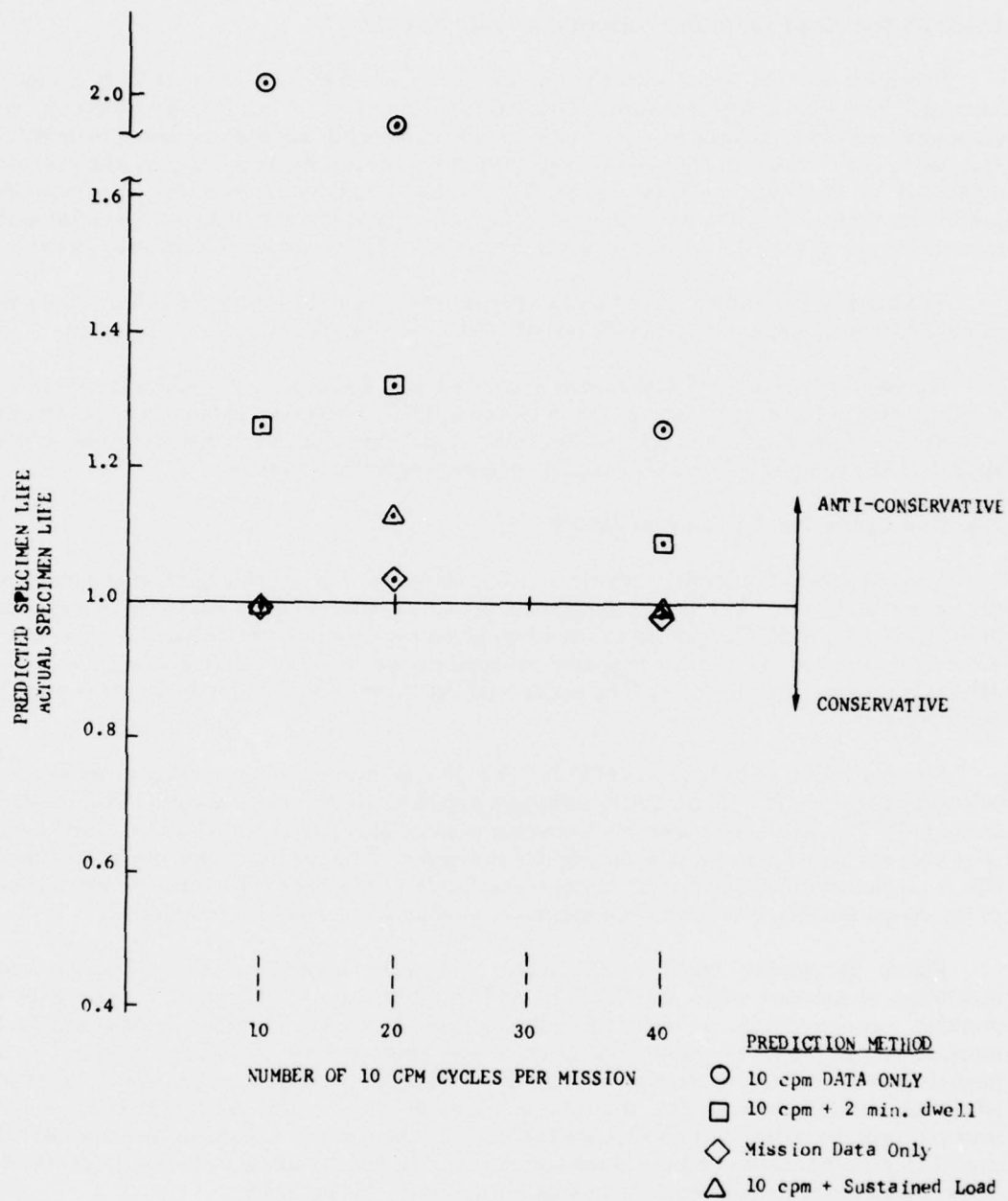*R = 0.1*

Figure 27. *Life Predictions for LCF-Dwell Interaction Test Specimens for IN-100, 1350°F, R = 0.1*

Major Load Excursion Influences on Crack Growth

Effect on Sustained Load Crack Growth at 1200° and 1350°F

Specimen 634 was tested with the mission shown schematically in figure 28 (2 minutes sustained load plus a 25% overload). To determine the effect of major load excursions on sustained load crack propagation, the da/dM vs ΔK relationship was first converted to da/dt vs K_{max} using the time per mission. Deviations from the measured da/dt vs K_{max} relationship are attributed to the major load excursions. To provide a tangible comparison, separate life predictions for specimen 634 were made using the pseudo da/dt and actual da/dt relationships. A comparison shows that the major load excursions retard 1200°F sustained load crack growth.

The linear superposition prediction for specimen 632, which saw repeated 25% overloads in combination with 2 minutes sustained load at 1350°F, was overly conservative, figure 29.

Figure 30 presents the SINH models that illustrate of effects of 25% and 50% repetitive overloads on sustained load crack growth in IN-100 at 1200°F. Figure 31 details the relationships between the SINH coefficients and overload ratio. This interpolative scheme was subsequently applied in the complex mission testing and analyses described in Reference 15.
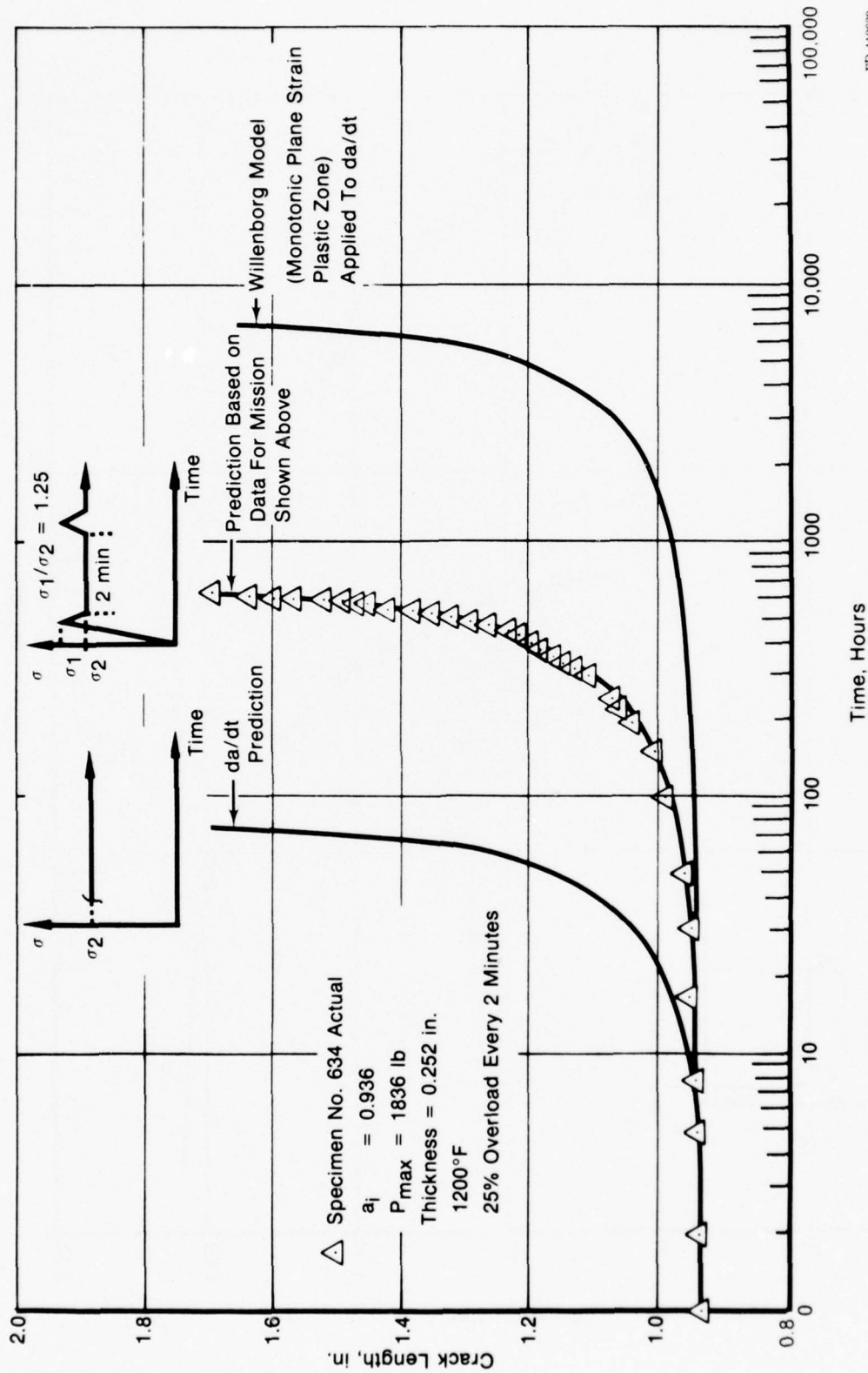
Effect on Cyclic Crack Growth at 1200°F

Specimen 666 was tested at 1200°F, R = 0.1, 10 cpm with a single major load excursion of 25% every 21st cycle. The life prediction using actual mission data was very accurate as illustrated in figure 32. The prediction based on linear superposition of damage (20 cycles at σ_2 + one cycle at σ_1) is conservative compared to actual results, as is the prediction based on cyclic data with constant amplitude σ_2. The major load excursions therefore produced crack growth retardation.

Specimen 669 was tested at 1200°F, R = 0.1, 10 cpm with a single major load excursion of 50% every 21 cycles. The life prediction using actual mission data was very accurate as illustrated in figure 33. The prediction based on linear superposition of damage (20 cycles at σ_2 + one cycle at σ_1 as in the actual mission) is a conservative estimation of crack propagation life for specimen 669. A prediction based on 10 cpm, constant amplitude (σ_2) data was also conservative relative to the actual mission. The major load excursions produced crack growth retardation.

Figure 34 presents crack growth curves comparing missions containing major load excursions to constant stress amplitude data. It is interesting to note that the 25 and 50% overload curves converge at stress intensities below 12 ksi$\sqrt{in}$. It might be expected that overload effects would be more pronounced at low applied stress intensities; however, it is possible that as the limiting crack growth rate for continuum propagation is approached, overload effects are minimized. Also note that above ΔK = 40 ksi$\sqrt{in}$., the effect of the 25% major load excursion is negligible. This suggests that there is some critical parameter that controls the transition from retardation effects to the accumulation of damage associated with the overload. Work is continuing to determine the qualitative nature of this parameter.

Figure 35 illustrates the effect of major load excursions on crack growth in IN-100, R = 0.5, 1200°F, overload ratio (OLR) of 1.5. Note that both retardant and accelerative effects can occur. Figures 36 and 37 present the interpolative synergistic SINH models for 25 and 50% repeated overloads respectively. Simple relationships are established between the SINH coefficients and OLR and cycles between overloads (figure 38). Table 5 summarizes the model.

This example illustrates that the SINH model is an effective empirical tool for developing accurate interpolative predictive schemes for complex spectra.

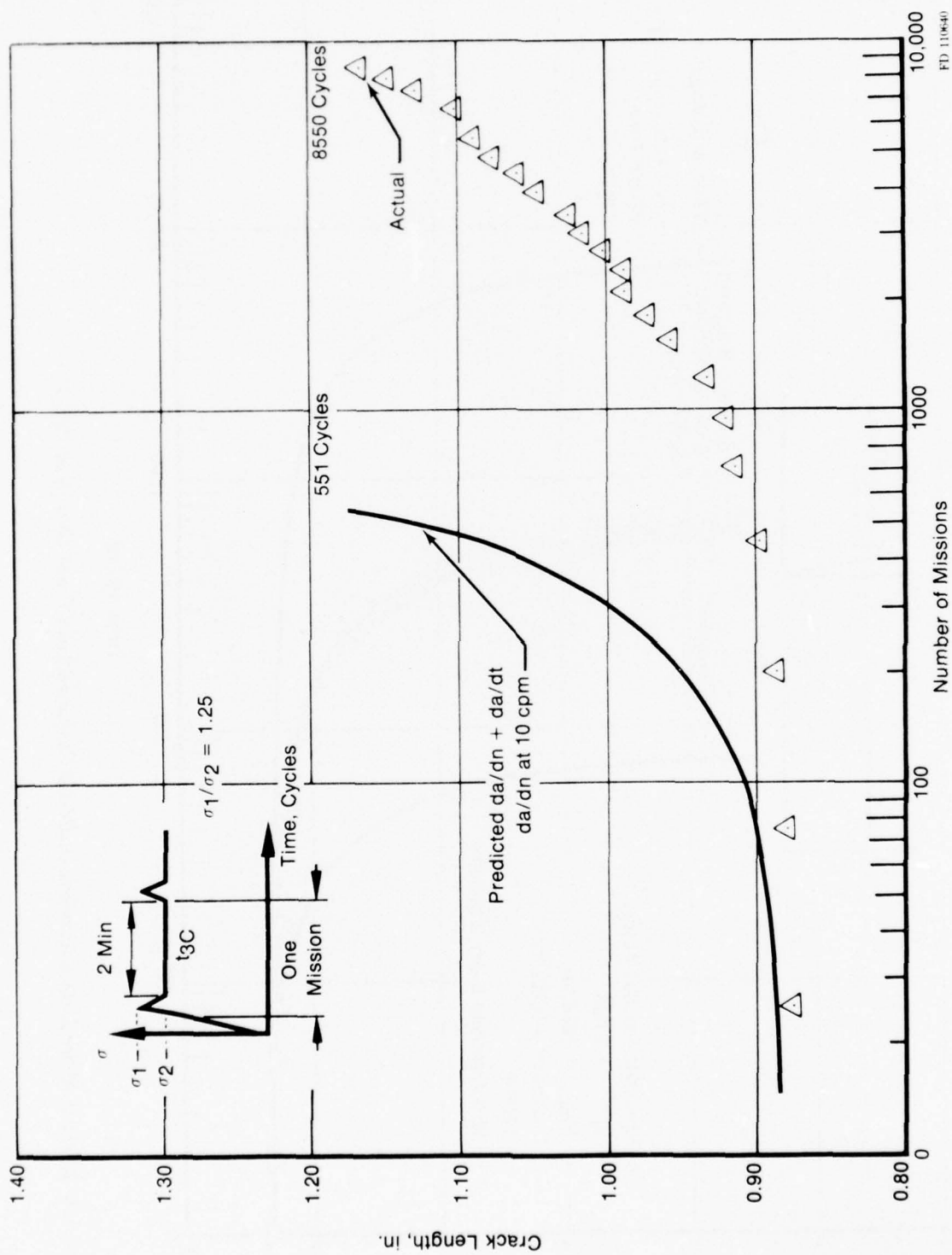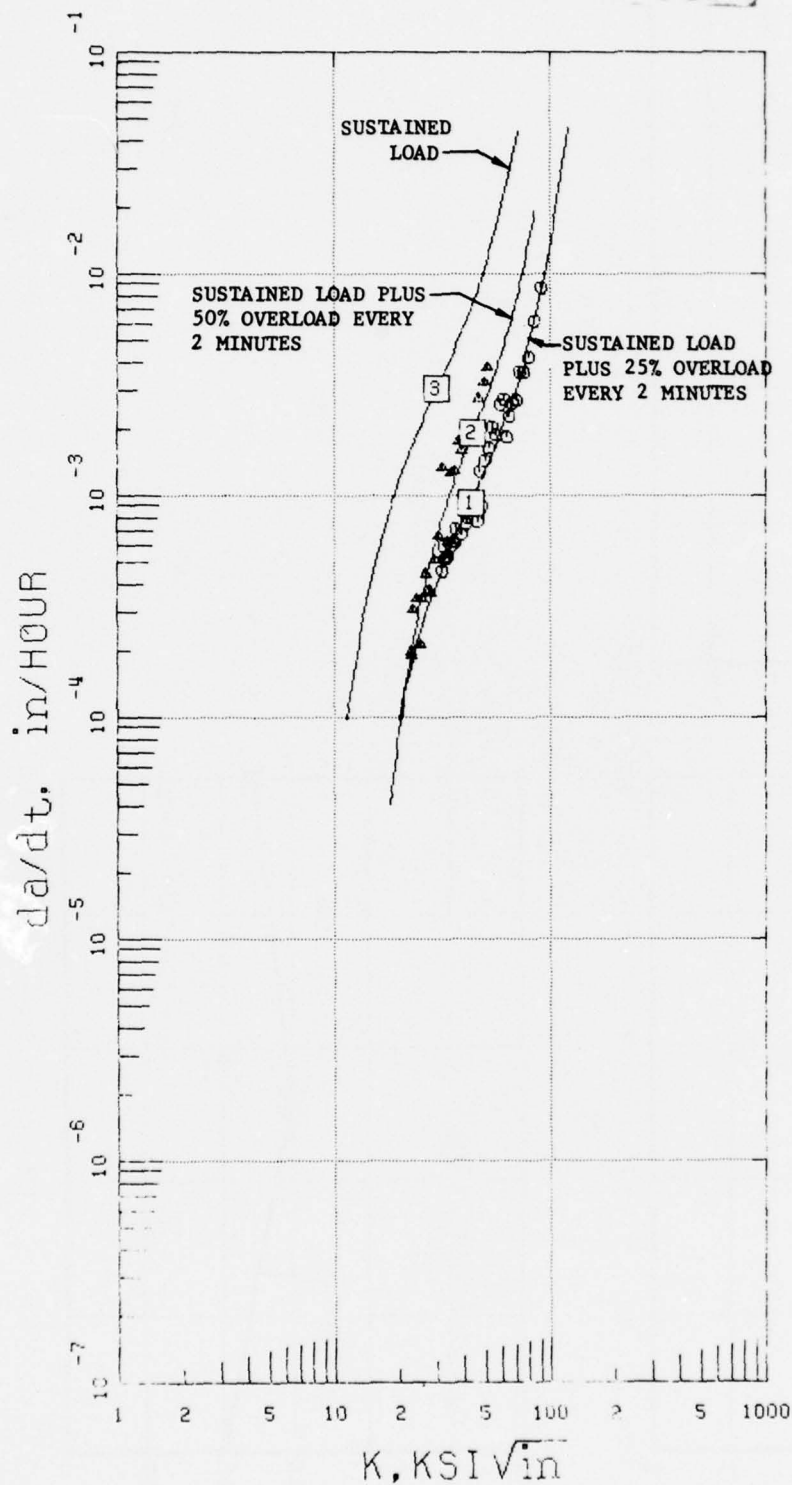Figure 28. *Effect of Major Load Excursions on IN-100 Sustained Load Crack Growth at 1200°F*

41

Figure 29. *Mission Mix (Overload) Life Prediction Using Linear Superposition, Specimen 632, IN-100, 1350°F*

FD 110640

42

Figure 30. *Effect of 25% and 50% Multiple Overloads on IN-100, 1200°F, Sustained Load Data*
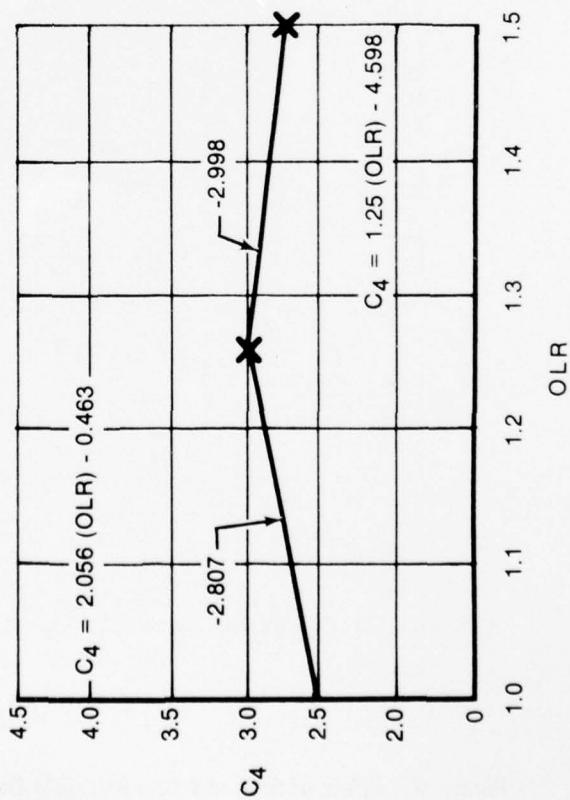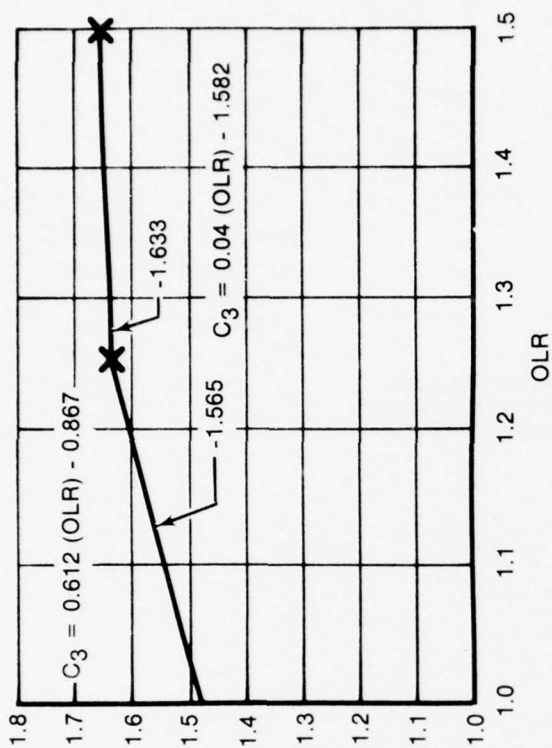
43

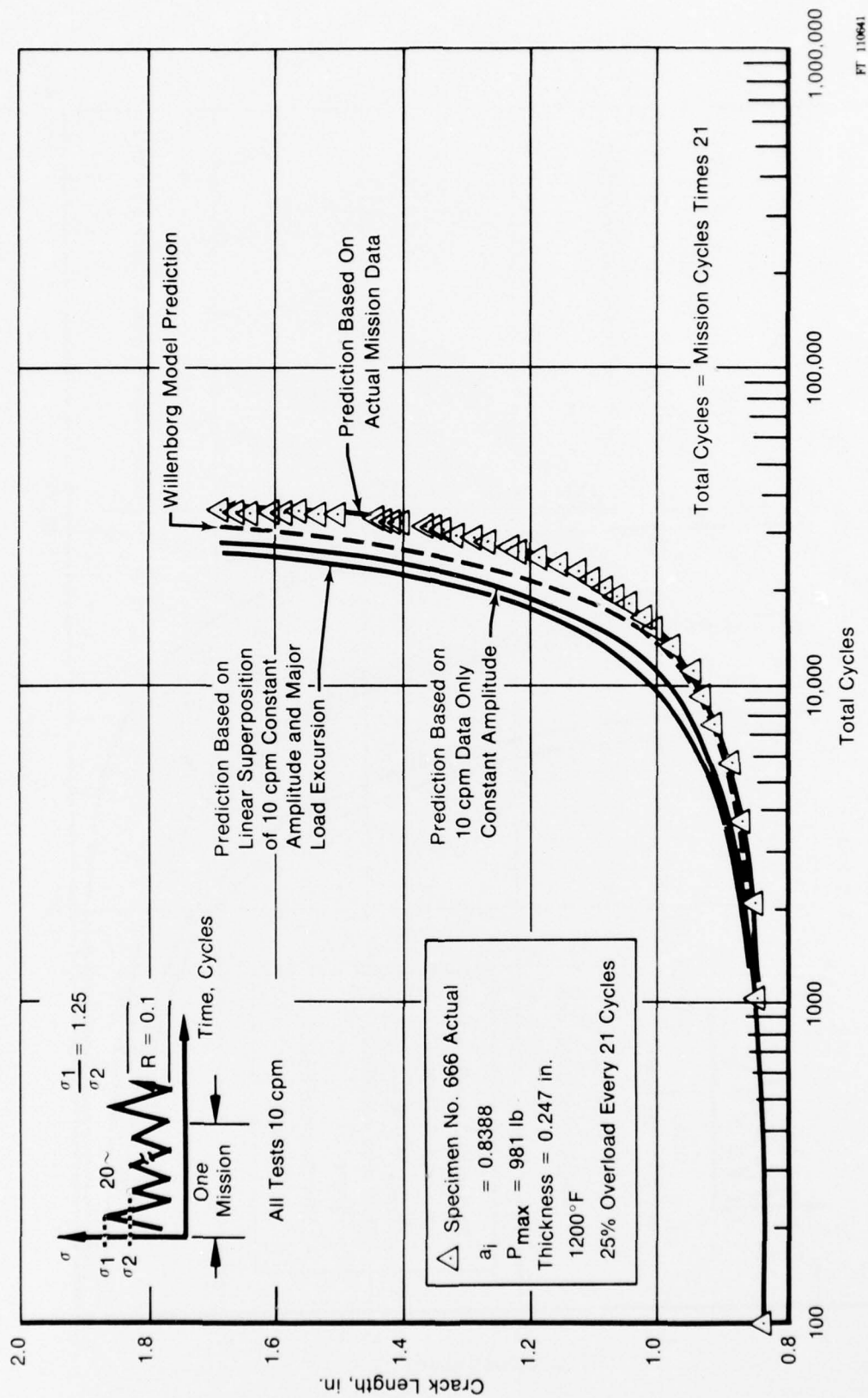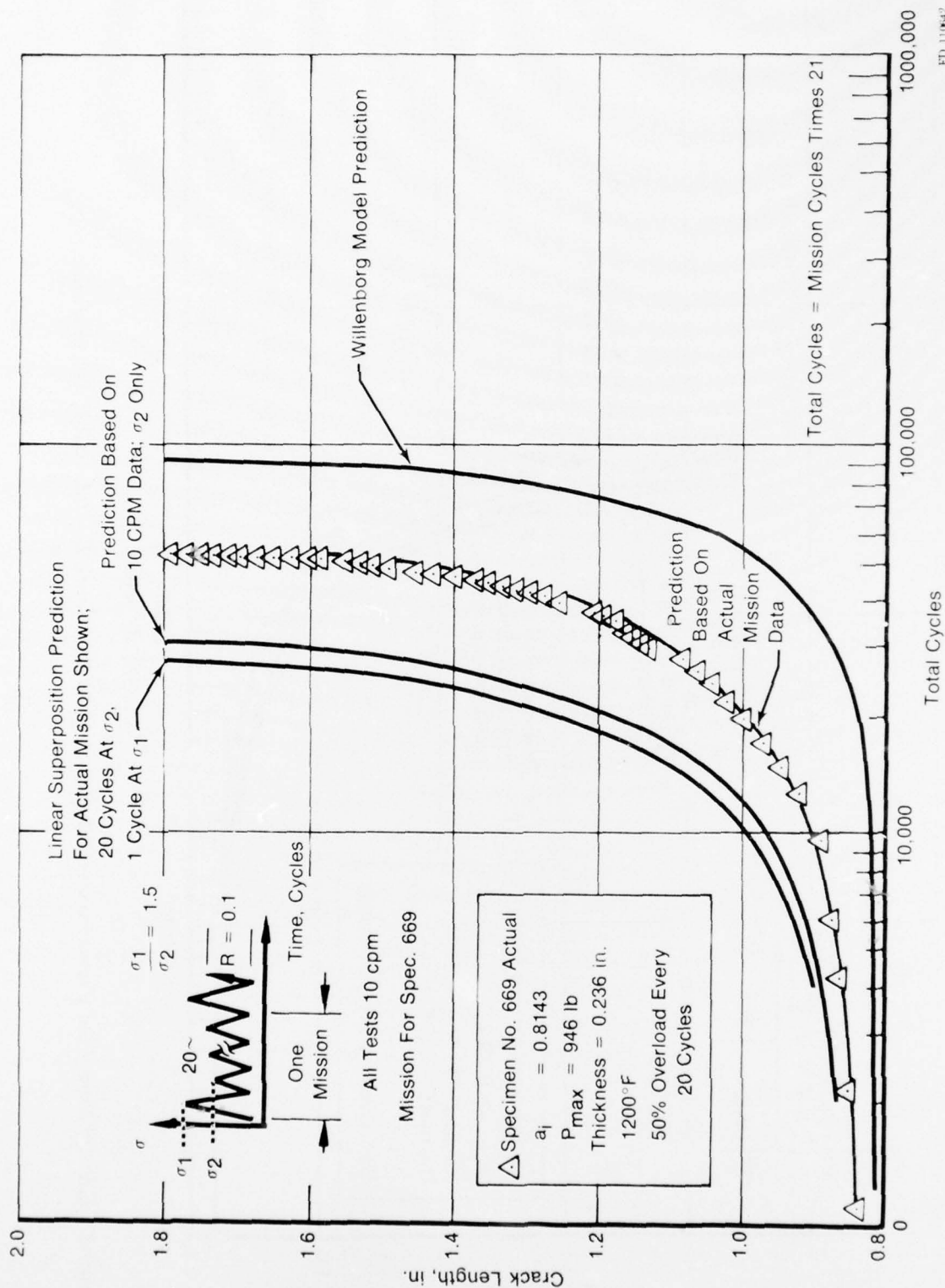Figure 31. Effect of Overload Ratio on Sinh Model Coefficients

44

FD 118671

Figure 32. Effect of Major Load Excursions on Crack Growth in IN-100, 10 cpm, R = 0.1, 1200°F, Life Predictions

45

FT 11061

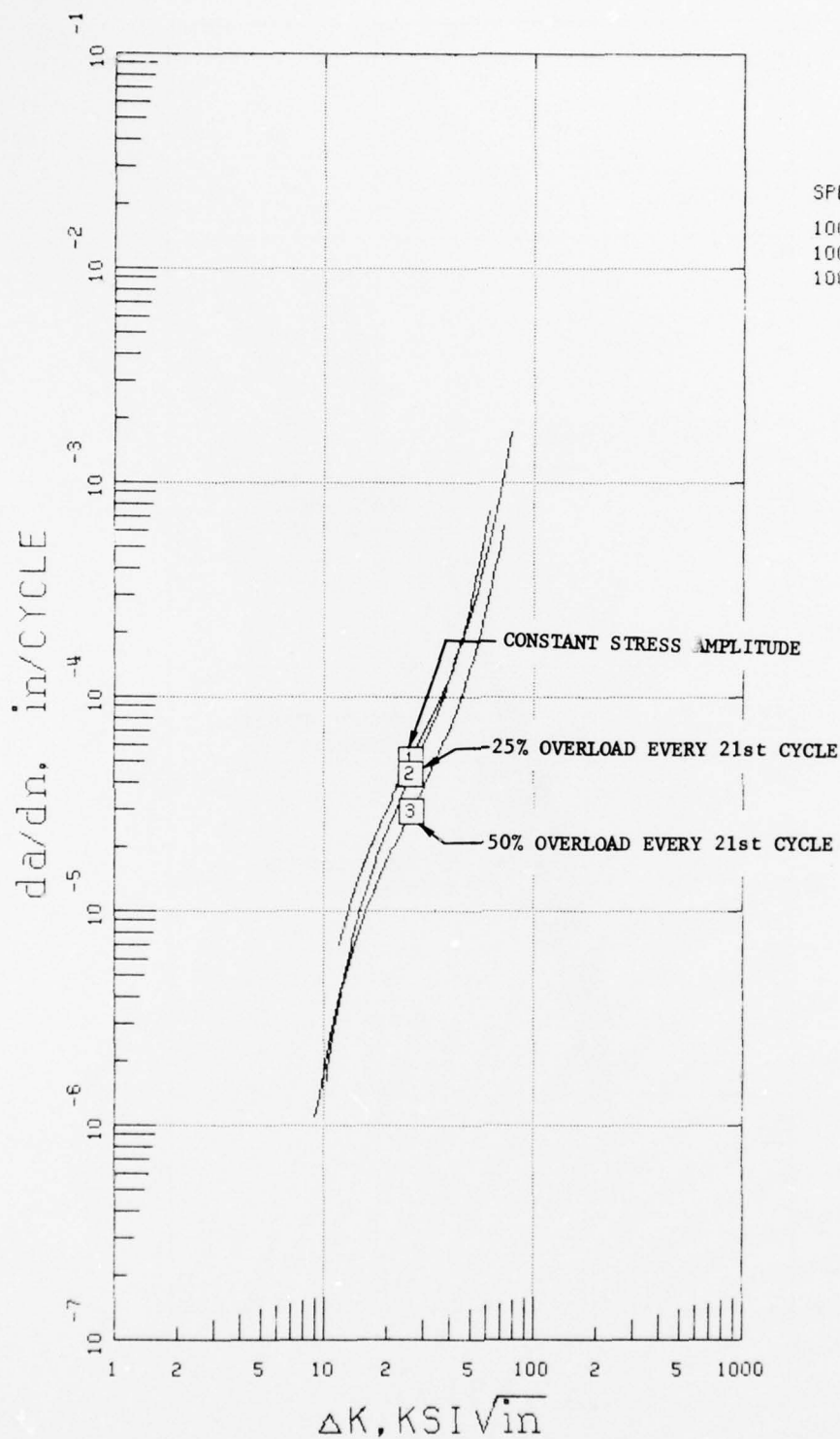Figure 33. *Effect of Major Load Excursions on Crack Growth in IN-100, 10 cpm, R = 0.1, 1200°F*

46

Figure 34. *Effect of Major Load Excursions on Crack Growth in IN-100, 10 cpm, R = 0.1, 1200°F, Data*
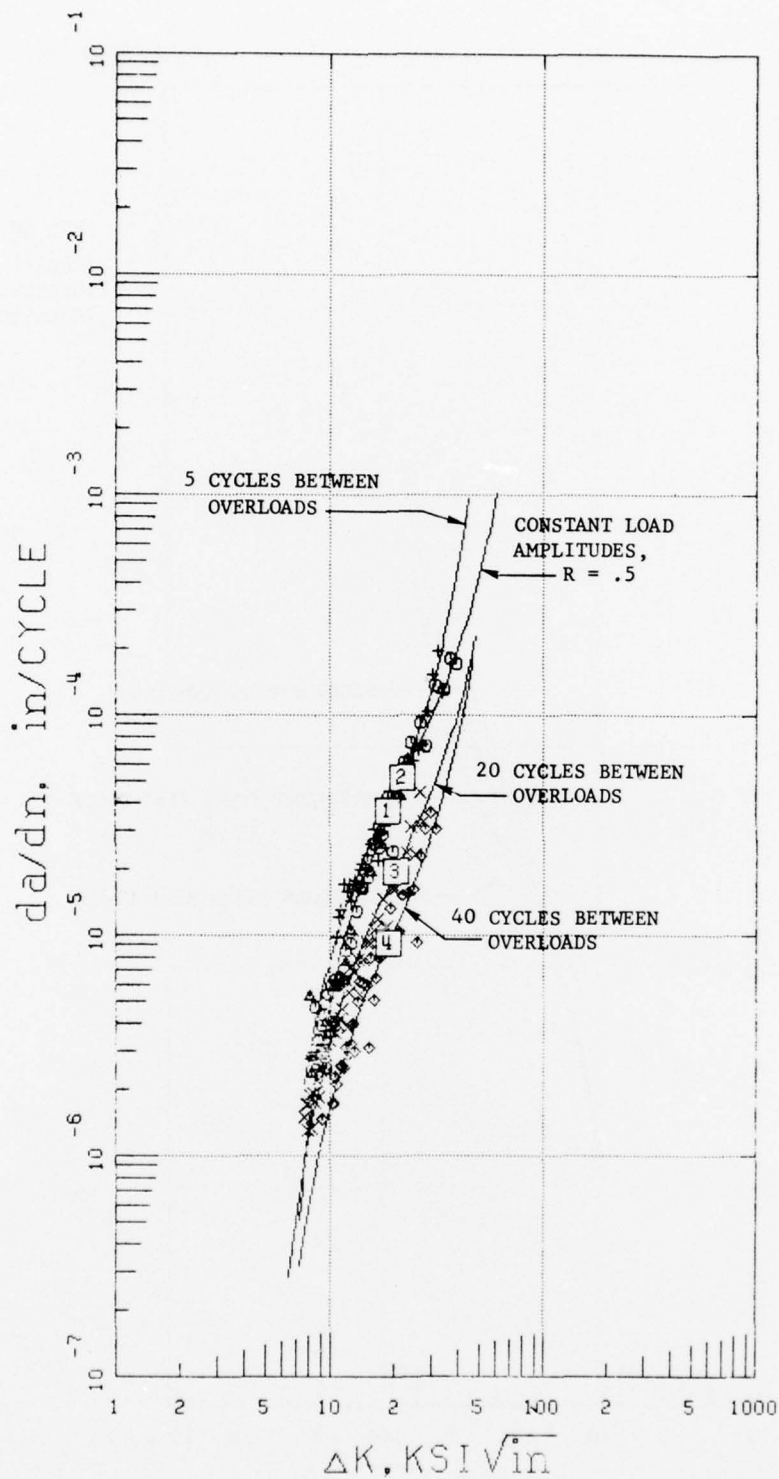
47

Figure 35. *Effect of Major Load Excursions on Crack Growth in IN-100, 1200°F, R = 0.5, OLR = 1.5*
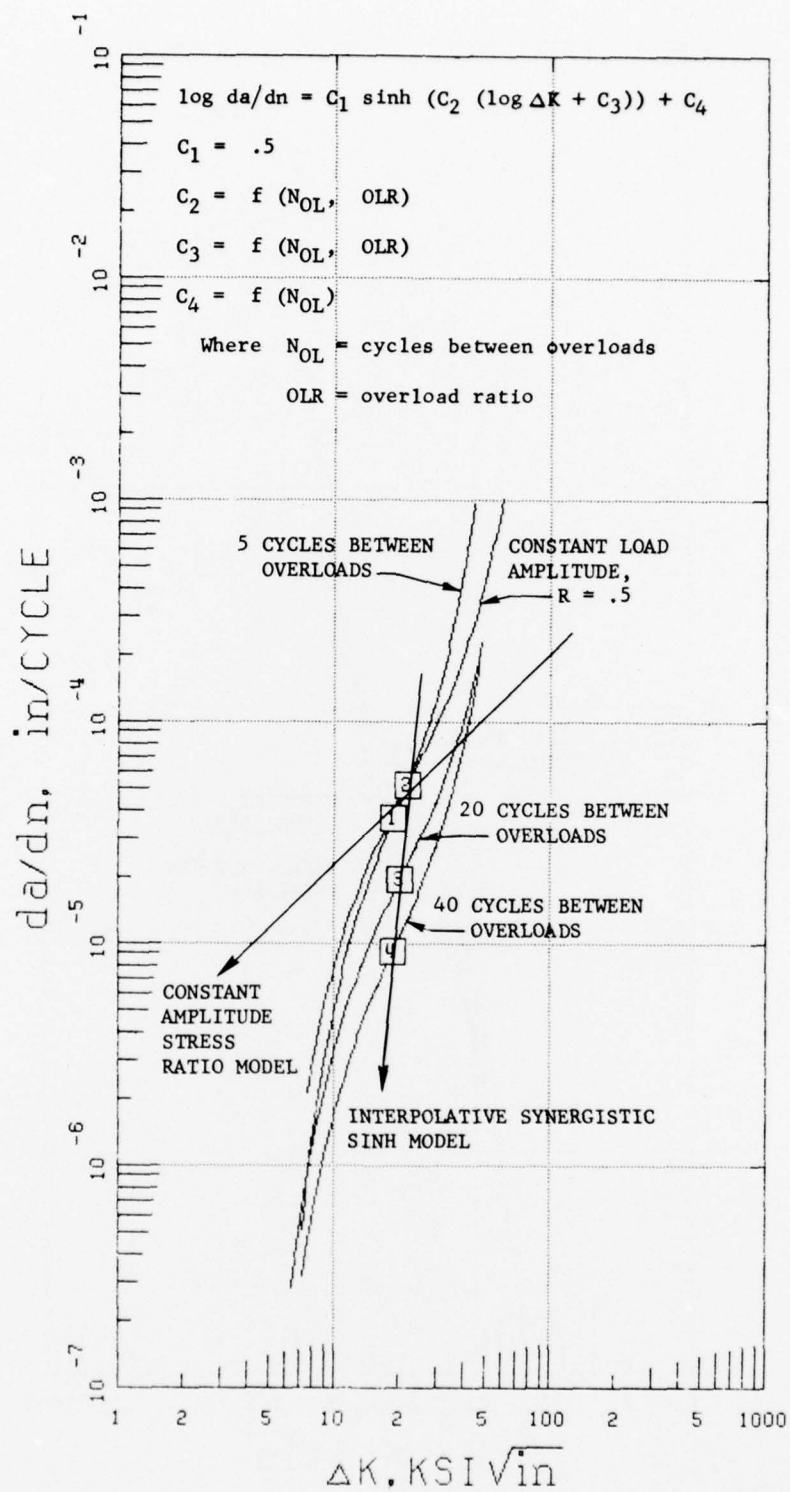
Figure 36. *Interpolative Synergistic Sinh Model, 1200°F, Overload Ratio = 1.5*
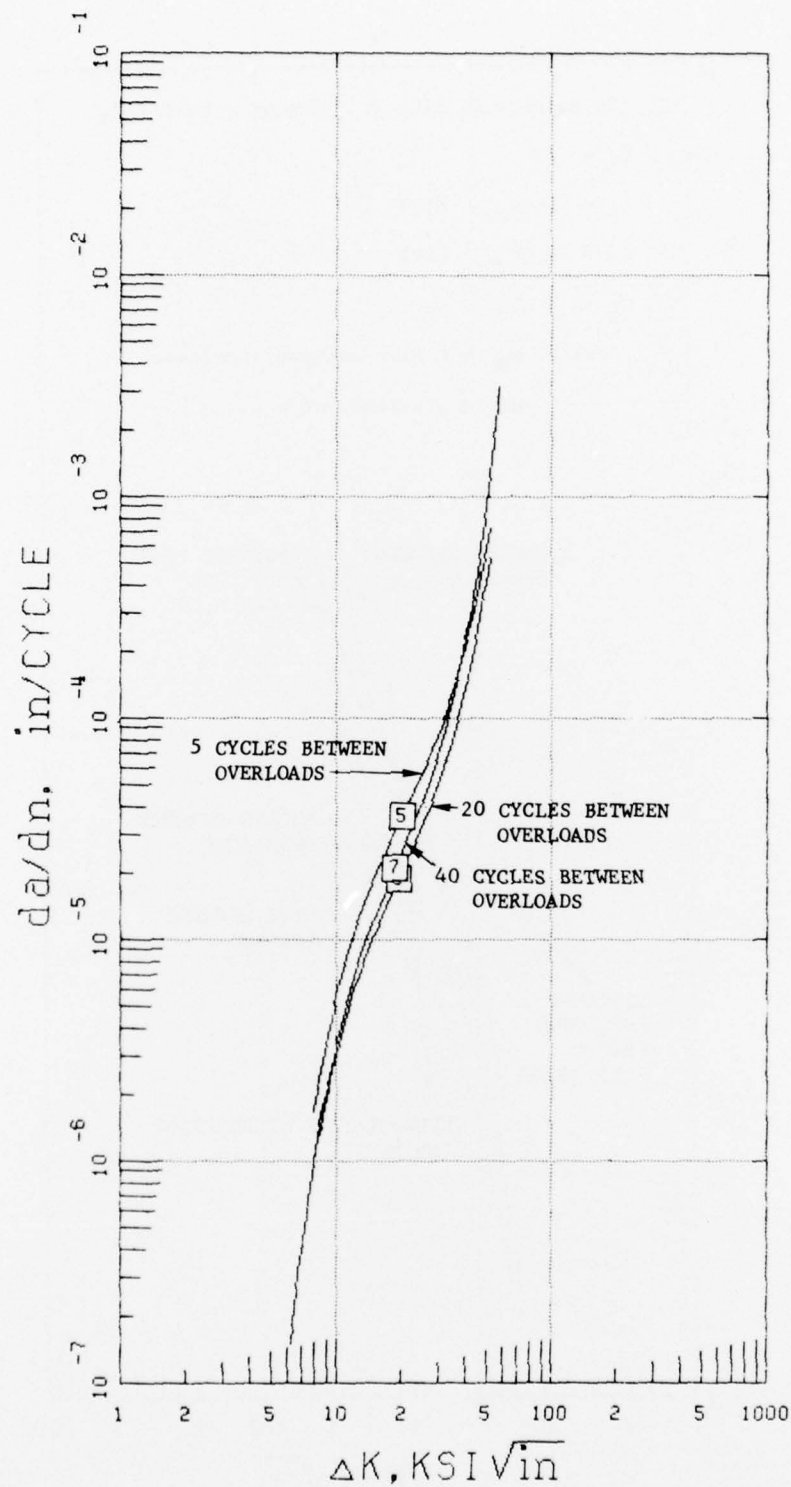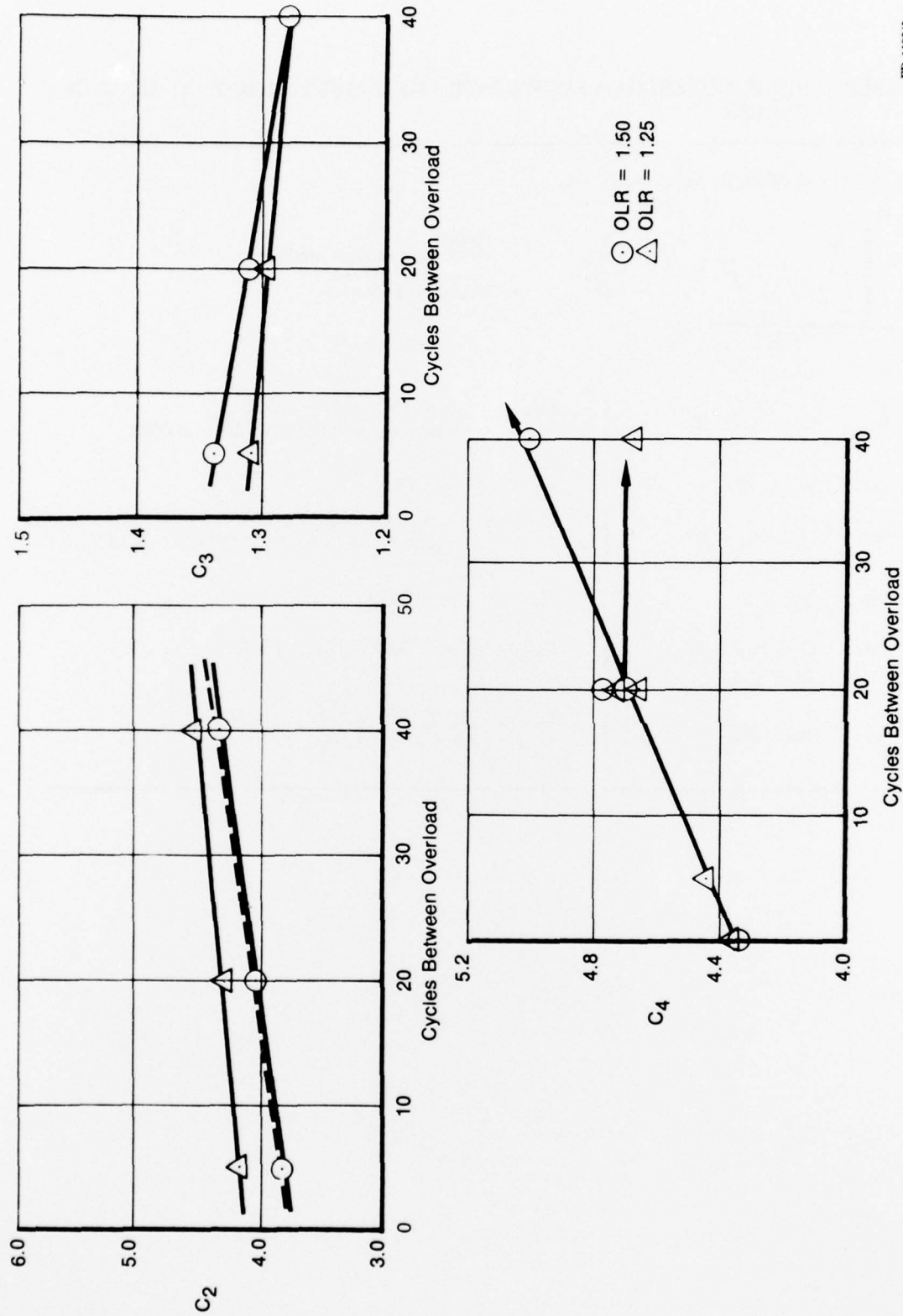
49

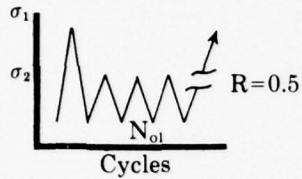Figure 37. *Interpolative Synergistic Sinh Model, 1200°F, Overload Ratio = 1.25*

50

Figure 38. *Effect Overload Ratio and Cycles Between Overloads on the Sinh Model Coefficients*

51

TABLE 5. SINGLE OVERLOAD SYNERGISTIC SINH MODEL 1200°F, R=0.5, 10 CPM CYCLES

$\log (da/dn) = C_1 \text{ SINH } (C_2 (\log \Delta K + C_3)) + C_4$

n	=	Cycles
N_{ol}	=	Cycles between single overloads
OLR	=	Overload ratio (σ_1/σ_2)
M	=	Missions = $n/(N_{ol} + 1)$

$C_1 \quad = 0.5$

for $\quad O \leq N_{ol} \leq 67 \qquad \Big\{ \quad C_2 \qquad = \theta_{C_2}(N_{ol} - 67) + 4.772$
$\qquad\qquad\qquad\qquad\qquad\qquad\qquad\qquad$ where $\theta_{C_2} = 0.0316 \, (\text{OLR}) - 0.0308$

for $\quad N_{ol} > 67 \qquad\qquad\quad C_2 \qquad = 4.772$

for $\quad O \leq N_{ol} \leq 40 \qquad \Big\{ \quad C_3 \qquad = \theta_{C_3}(N_{ol} - 40) - 1.279$
$\qquad\qquad\qquad\qquad\qquad\qquad\qquad\qquad$ where $\theta_{C_3} = (3.48 \times 10^{-3}) \, \text{OLR} - (3.475 \times 10^{-3})$

for $\quad N_{ol} > 40 \qquad\qquad\quad C_3 \qquad = -1.279$

for $\quad O \leq N_{ol} \leq 20 \qquad \Big\{ \quad C_4 \qquad = -0.0173 \, N_{ol} - 4.345$
$\qquad$ OLR ≤ 1.5

for $\quad N_{ol} > 20 \qquad\qquad \Big\{ \quad$ OLR ≥ 1.5; $C_4 = 0.0173 \, N_{ol} - 4.345$
$\qquad\qquad\qquad\qquad\qquad\qquad\quad$ OLR < 1.5; $C_4 = -4.700$

Effect on Cyclic Crack Growth at 1350°F

Specimens 661, 662, and 664 were tested at 1350°F, R = 0.8, and ν = 20 cps with major load excursions every 41st cycle. Specimen 662 experienced a 25% sawtooth load excursion, specimen 661 a 50% sawtooth load excursion, whereas specimen 664 was held at elevated load (50% excursion) for two minutes before returning to the lower load for 40 cycles.

Figure 39 illustrates that major load excursions at this temperature (1350°F) have a detrimental effect on crack growth rates, with the greater effect being at the higher overload ratio. It is also shown that the imposition of a 2-minute dwell further accelerates crack growth rate. It is interesting to note that the effect of overload for constant cycles between overloads results in a model similar to that for stress ratio developed in Section III. For the 50% excursion, a comparison of 10 cpm ramp rates and the 2-minute dwell reveals a model similar to that for temperature in Section III. Here, the correlation line is vertical, i.e., C_3 is constant.

Specimens 661 and 664 were also analyzed to assess the applicability of linear superposition to mission life prediction at 1350°F. Figure 40 presents an anlysis for specimen 661. Although the load excursion was applied at 10 cpm with an exact stress ratio of 0.6, data for R = 0.5 was used for computational purposes because of its proximity to the actual value since a stress ratio model was not developed for 1350°F. This prediction, and that based on the actual mission data, resulted in accurate ($N_{predicted}/N_{actual} = 0.92_{superposition}, = 1.05_{mission}$) estimations of specimen life as well as following the true shape of the a-M curve.

Figure 41 presents an analysis for specimen 664. The actual excursion stress ratio was R = 0.6 at a frequency of 10 cpm. Crack propagation characterizations for both 10 cpm, R = 0.5 and sustained load were used to represent the 2 minutes at increased load. This prediction was inaccurate when compared to the mission life analysis using the actual mission data ($N_{actual} = 1.02_{mission}, = 1.341_{superposition}$).

Interpolative empirical models for complex spectra based on the SINH model show considerable promise. The utilitarian value of some of the models developed in this section are demonstrated in Reference 15 where cumulative damage analyses are performed for simulated engine missions.
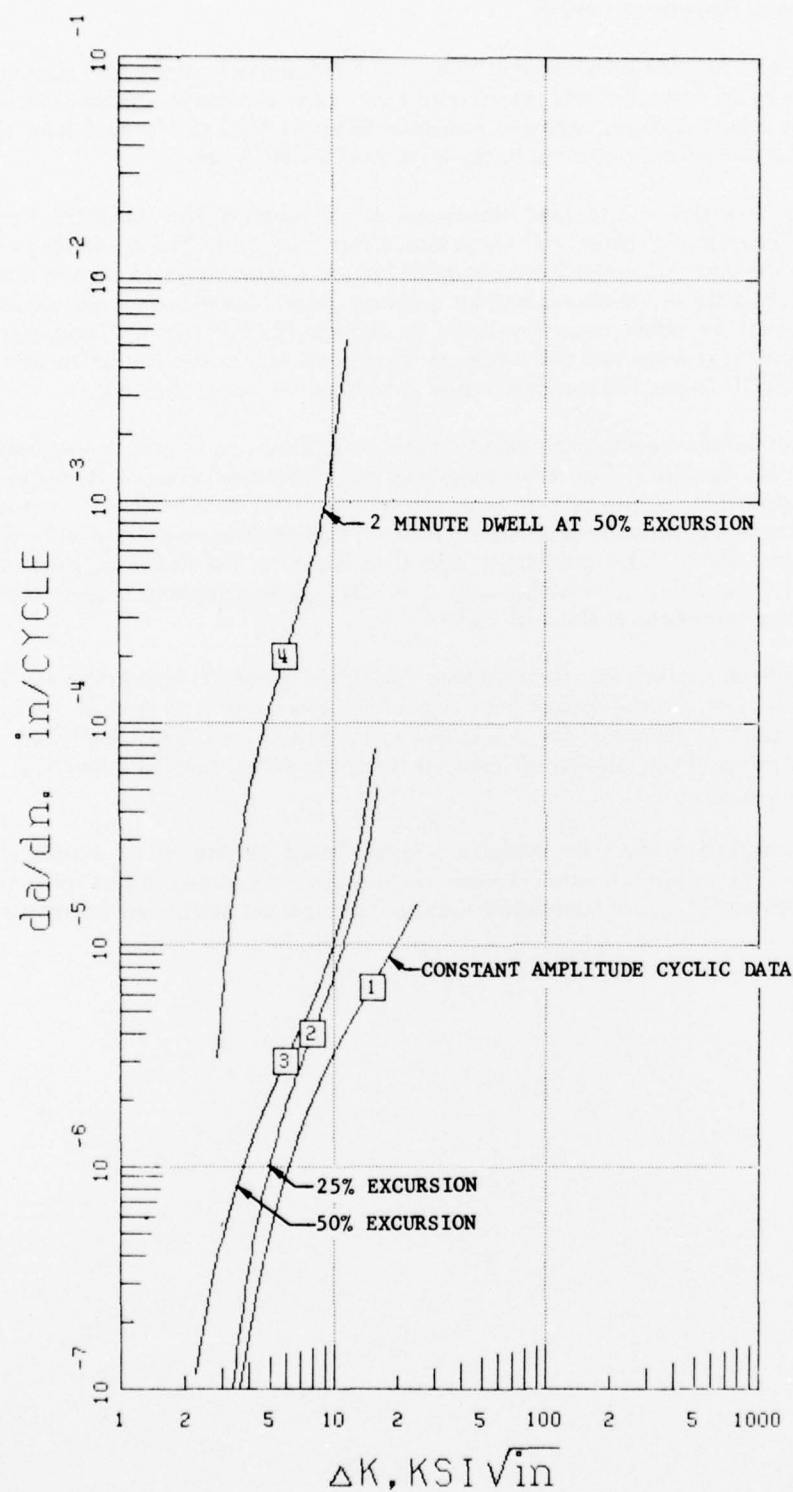
Figure 39. Effect of Major Load Excursions on Crack Growth in IN-100, 1350°F, R = 0.8, 20 cps, Data

54
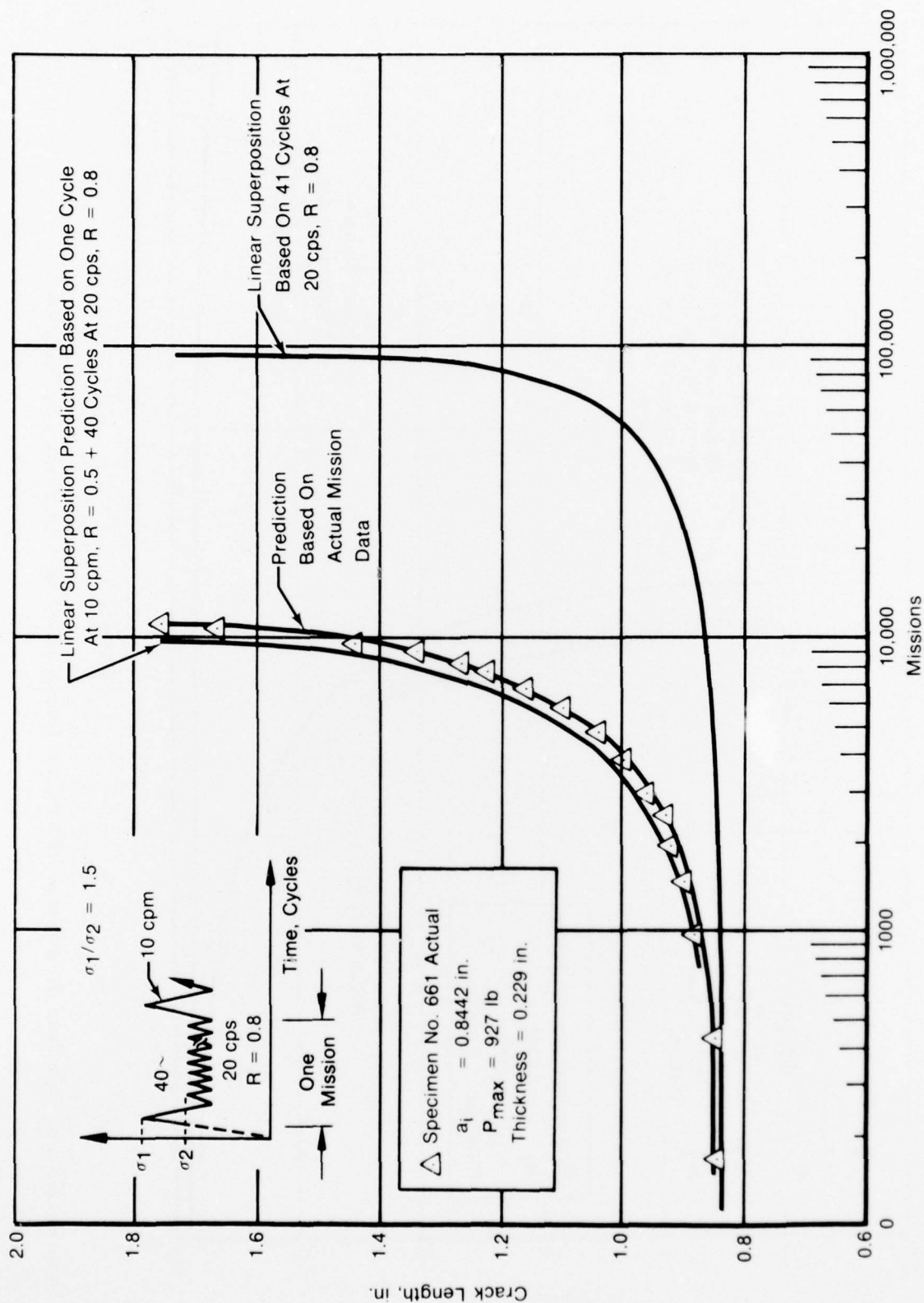
Figure 40. *Effect of Major Load Excursions on IN-100 Crack Growth, 1350°F, R = 0.8, 20 cps, Life Predictions*

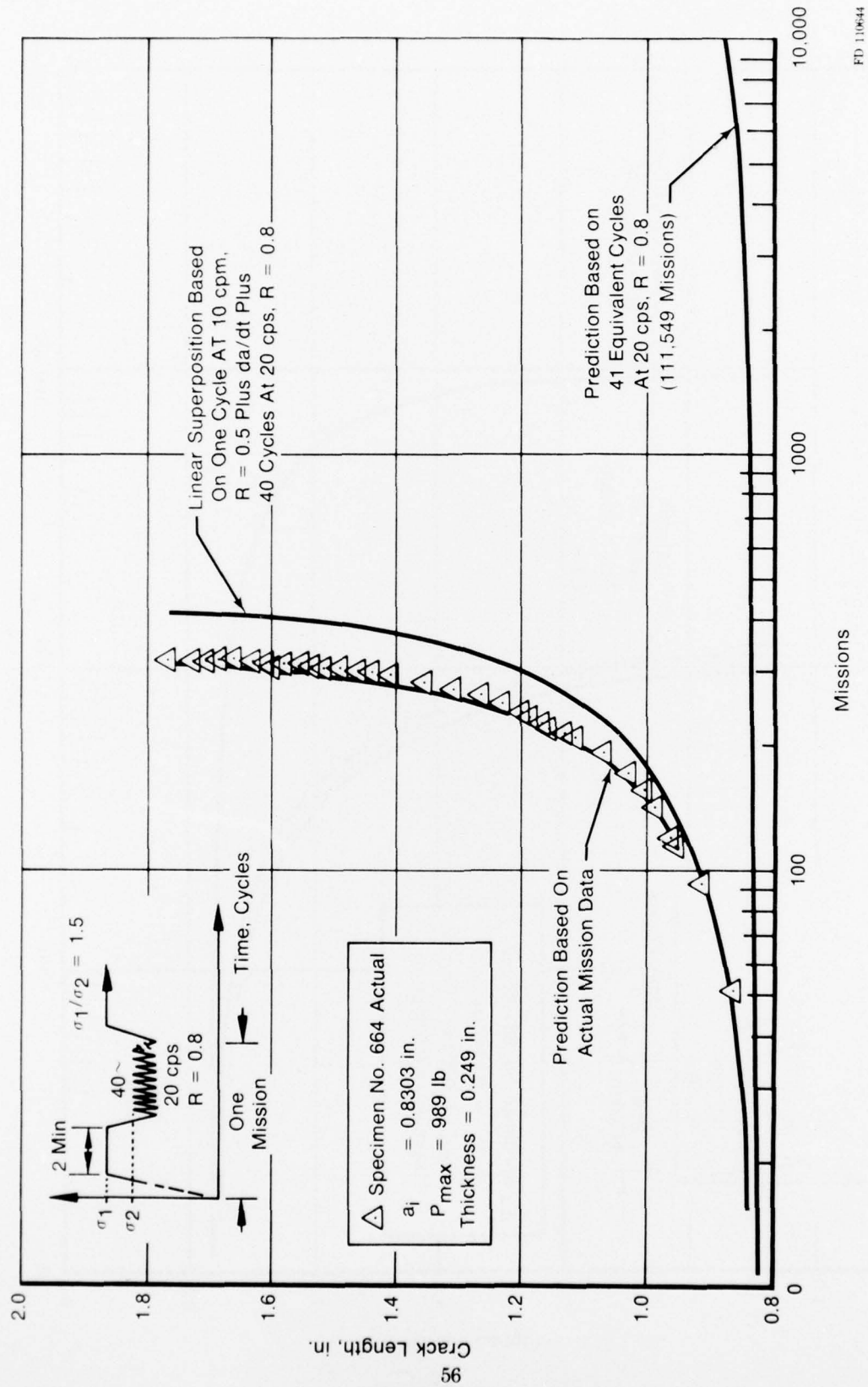FD 110643

Figure 41. *Effect of Major Load Excursions on IN-100 Crack Growth, 1350°F, R = 0.8, 20 cps, Life Predictions*

56

FD 110644

SECTION V
CONCLUSIONS

The applicability of Linear Elastic Fracture Mechanics (LEFM) for predicting high-temperature crack growth in a gas turbine disk alloy, IN-100, is investigated. The following conclusions are presented.

1. At room temperature LEFM is not generally applicable to predicting crack growth in IN-100 because of large-scale crack tip inelasticity.

2. At elevated temperature (T > 1000°F), LEFM can be used to predict crack propagation behavior because oxidation reduces crack tip inelasticity. However, caution must be exercised to assure that plane strain constraints are met.

    a. The effect of specimen thickness is a function of cyclic conditions and temperature.

    b. The effect of net section stress is a function of cyclic conditions.

3. Major load excursions can cause either retardation or acceleration depending on operating conditions.

4. The analysis of IN-100 crack propagation data at elevated temperatures is based on the hyperbolic sine model

$$\log (da/dn) = C_1 \sinh (C_2 (\log (\Delta K) + C_3)) + C_4,$$

the coefficients of which are shown to be simply related to test frequency, stress ratio, and temperature.

5. Interpolative empirical models for complex spectra have been developed using the SINH model. These models show considerable promise as an accurate means for the prediction of crack growth at elevated temperature under representative engine operating conditions (see Reference 15).

REFERENCES

1. Hill, R. J., "Report with Recommendations on Turbine Engine Component Fatigue Life Prediction," Air Force Materials Laboratory, Wright -Patterson Air Force Base, December 1974.

2. Wallace, R. M., C. G. Annis, and M. C. VanWanderham, "An Experimental Procedure for the Accurate Prediction of Total LCF Life," presented at ASM Materials Science Symposium, Cincinnati, Ohio, November 1975, P&WA GP 75-175.

3. "Experimental Procedure for the Prediction of Engine Disk Residual Life Using Acoustic Emission Techniques," Pratt & Whitney Aircraft FP 75-208, 15 September 1975, AFML Contract F33615-76-C-5172.

4. Wallace, R. M., C. G. Annis, D. L. Sims, "Application of Fracture Mechanics at Elevated Temperatures," Pratt & Whitney Aircraft FR-7506, March 1976.

5. Nikbin, K. M., G. A. Webster, and C. E. Turner, "Relevance of Nonlinear Fracture Mechanics to Creep Cracking," *Cracks and Fracture*, ASTM STP 601, American Society for Testing and Materials, 1976, pp. 47-62.

6. Hutchinson, J. W., Journal of Mechanics and Physics of Solids, Vol. 16, 1968, p. 13-31.

7. Landes, J. D., and J. A. Begley, "A Fracture Mechanics Approach to Creep Crack Growth," *Mechanics of Crack Growth*, ASTM STP 590, American Society for Testing and Materials, 1976, pp. 128-148.

8. Gell, M. and G. R. Leverant, "Mechanisms of High-Temperature Fatigue," Fatigue at Elevated Temperatures, ASTM STP 520, American Society for Testing and Materials, 1973, pp. 37-67.

9. Wallace, R. M., M. C. VanWanderham, "Investigation of Fatigue Crack Propagation in Ti 6246 and IN-100 Using Acoustic Emission Techniques," P&WA GP 74-136.

10. Mucci, J., "Fracture Toughness of P&WA 1058 Using the J-Integral Techniques," FMDL 19598, 11/3/76.

11. Annis, C. G., and M. C. VanWanderham, Monthly TR No. 10, Contract F33615-75-C-5097, P&WA FR-7559, 15 April 1976.

12. P&WA Inter-Office Correspondence, Gemma, et.al. to Cruse, 10 September 1975.

13. Aurich, D., "The Influence of Stress State on the Plastic Zone Size," Engineering Fracture Mechanics, 1975, Vol. 7, pp. 761-765.

14. Annis, C. G., R. M. Wallace, D. L. Sims, "An Interpolative Model for Elevated Temperature Fatigue Crack Propagation," Air Force Materials Laboratory, AFML-TR-76-176, April 1977.

15. Sims, D. L., C. G. Annis, R. M. Wallace, "Cumulative Damage Fracture Mechanics at Elevated Temperatures," Air Force Materials Laboratory AFML-TR-76-176 Part III, April 1977.

16. Willenborg, J., R. M. Engle, and H. A. Wood, "A Crack Growth Retardation Model Using an Effective Stress Concept," Tech Mem. 71-1-FBR, January 1971.